Bioactive Materials 16 (2022) 433–450

Contents lists available at ScienceDirect

Bioactive Materials

journal homepage: www.keaipublishing.com/en/journals/bioactive-materials

Anti-Sca-1 antibody-functionalized vascular grafts improve vascular regeneration via selective capture of endogenous vascular stem/progenitor cells

He Wang, Mengmeng Xing, Weiliang Deng, Meng Qian, Fei Wang, Kai Wang, Adam C. Midgley **, Qiang Zhao *

State Key Laboratory of Medicinal Chemical Biology, Haihe Laboratory of Sustainable Chemical Transformations, Key Laboratory of Bioactive Materials (Ministry of Education), Frontiers Science Center for Cell Responses, College of Life Sciences, Nankai University, Tianjin, China

ARTICLE INFO

Keywords:
Small-diameter vascular grafts
Surface modification
Stem cell antigen-1 (Sca-1) antibody
Vascular stem/progenitor cells (SPCs)
Tissue regeneration

ABSTRACT

Small-diameter vascular grafts fabricated from synthetic biodegradable polymers exhibit beneficial mechanical properties but often face poor regenerative potential. Different tissue engineering approaches have been employed to improve tissue regeneration in vascular grafts, but there remains a requirement for a new generation of synthetic grafts that can orchestrate the host response to achieve robust vascular regeneration. Vascular stem/progenitor cells (SPCs) are mostly found in quiescent niches but can be activated in response to injury and participate in endothelium and smooth muscle regeneration during neo-artery formation. Here, we developed a functional vascular graft by surface immobilization of stem cell antigen-1 (Sca-1) antibody on an electrospun poly(ε-caprolactone) graft (PCL-Sca-1 Ab). PCL-Sca-1 Ab promoted capture and retainment of Sca-1$^+$ SPCs *in vitro*. In rat abdominal aorta replacement models, PCL-Sca-1 Ab stimulated *in vivo* recruitment of Sca-1$^+$ SPCs, and drove SPCs differentiation towards vascular cell lineages. The origin of infiltrated Sca-1$^+$ SPCs was further investigated using a bone marrow transplantation mouse model, which revealed that Sca-1$^+$ SPCs originating from the resident tissues and bone marrow contributed to rapid vascular regeneration of vascular grafts. Our data indicated that PCL-Sca-1 Ab vascular grafts may serve as a useful strategy to develop next generation cell-free vascular grafts.

1. Introduction

Cardiovascular diseases (CVDs) are the leading cause of morbidity and mortality among the major noncommunicable diseases [1]. An estimated 17.9 million people died from CVDs in 2019, according to a 2021 report published by the World Health Organization. The treatment of occluded or damaged coronary arteries typically involves bypass surgery using autologous arteries and veins [2]. However, the clinical applications of autologous arteries and veins are limited due to lack of availability, often complicated by pre-existing disease and size mismatches in a sizeable percentage of patients [3–6]. Hence, vascular substitutes constructed from synthetic biodegradable polyesters have emerged as a burgeoning research field in recent years. Artificial vascular grafts have demonstrable success when used as replacements for large diameter vessels [7], but they have been generally proven inadequate when used as small diameter (<6 mm) arterial grafts, owing to poorly orchestrated tissue formation, the onset of thrombosis, and incidence of severe neointimal hyperplasia [8]. To improve the performance of artificial small-diameter vascular grafts, considerations of capabilities of the material to induce tissue regeneration *in situ* for the rapid integration with host tissue and formation of functional blood vessels is imperative to achieve long-term patency. Rapid endothelialization [9], regeneration of contractile smooth muscle layers (SMCs) [10], and prolonged modulation of inflammation *in vivo* may be effectively achieved through the design of cell-free vascular grafts that invoke the host's own regenerative potential, to orchestrate cell responses and promote extracellular matrix (ECM) deposition and remodelling [11].

Peer review under responsibility of KeAi Communications Co., Ltd.
* Corresponding author.
** Corresponding author.
E-mail addresses: midgleyac@nankai.edu.cn (A.C. Midgley), qiangzhao@nankai.edu.cn (Q. Zhao).

https://doi.org/10.1016/j.bioactmat.2022.03.007
Received 22 December 2021; Received in revised form 18 February 2022; Accepted 4 March 2022
Available online 10 March 2022

Recent studies have reported tissue regeneration of functional arteries initiated by cell-free grafts [12–15]. The modification of various biological compounds and biomolecules onto scaffolds can endow functionalization with grafts to elicit specific biological actions and improve cellularization, tissue remodelling, and patency [16]. Such modifications include the incorporation of vascular effector molecules (e.g., nitric oxide, NO; NO donors) [17,18], growth factors or cytokines (e.g., vascular endothelial growth factor, VEGF) [19,20] and peptides (e.g., integrin binding motif, RGD) [21]. Despite advantages gained by functionalization of vascular grafts with growth factors, their sensitivity to degradation within proteolytic tissue microenvironments and relative difficulty of synthesis, purification and incorporation into scaffold materials, ultimately limit widespread application of growth factor-functionalized vascular grafts. Hence, alternative protein-based candidates include antibodies, which have greater stability, and can more readily be produced and incorporated into vascular grafts. Antibodies are of particular interest due to their capability to recognize antigen-presenting cells, and have led to the generation of biomaterials that can capture and recruit target cells to improve cellularization of the scaffold, leading to enhanced tissue regeneration [9,22–25].

Accumulating evidence has established the active role of vascular stem/progenitor cells (SPCs) in vascular homeostasis and remodelling [26–28]. SPCs distributed in bone marrow and blood vessel walls are a heterogeneous population of cells. The majority express the marker, stem cell antigen-1 (Sca-1), and subpopulations have been identified that express C-Kit and CD34 [29]. It was shown that Sca-1$^+$ SPCs possess bi-lineage potential, meaning they can differentiate into specific vascular cell lineages, including endothelial cells (ECs) and smooth muscle cells (SMCs), both *in vitro* and *in vivo* [30–32]. Circulating SPCs present in the bloodstream can be recruited to the vascular wall to differentiate into ECs, SMCs, or other cells in response to certain stimuli, which is suggested to contribute to the restoration of the endothelium, smooth muscle layers, and vascular regenerative processes [28]. Hence, the favourable capacity of Sca-1$^+$ SPCs could be exploited for useful applications in tissue engineering of artificial vascular grafts [33].

Surface modification is being increasingly utilized to immobilize bioactive macromolecules onto scaffolds, to improve biocompatibility, hemocompatibility, and cell-substrate interactions. Surface modification technology using biotin-avidin conjugation systems has the advantages of facile preparation, retainable activity of conjugated biomacromolecules, and adaptability to molecules with a wide range of shapes and sizes. Due to the highly specific and strong affinity interactions between biotin and avidin, the binding reaction is fast, irreversible, and has stability that persists under a range of acidities, temperatures, and within organic solvents. Importantly, the nature of high-affinity antibody-antigen interactions presents different binding kinetics than cell adhesion molecules, and in the case of cell capture, these interactions mediate the firm arrest of desired cells from dynamic flow to the modified substrate surface [34]. In this work, we fabricated poly(ε-caprolactone) (PCL) microfiber vascular grafts by electrospinning and immobilized anti-Sca-1 antibodies onto PCL microfibers using the biotin-avidin system. The obtained anti-Sca-1 antibody-functionalized PCL vascular grafts (PCL-Sca-1 Ab) were evaluated for cell recruitment, capture, and retainment under static and dynamic flow *in vitro* culture conditions, followed by assessment of regenerative potential and vascular compliance in rat abdominal aorta replacement models. In addition, a bone marrow transplantation carotid artery replacement mouse model was employed to obtain further insights into the origin and differentiation of the recruited Sca-1$^+$ SPCs, and whether they were predominantly recruited from resident tissues or bone marrow. Our data suggested that anti-Sca-1 antibody presentation significantly increased Sca-1$^+$ SPC capture and retention in cell-free PCL scaffolds, which led to effective and enhanced vascular regeneration.

2. Materials and methods

2.1. Materials

Poly(ε-caprolactone) (PCL80K, M_w = 80000), oligomer poly(ε-caprolactone)-diol (PCL2K-diol) (M_n = 2000), 4′-Hydroxyazobenzene-2-carboxylic acid (HABA), biotin, and avidin were purchased from Sigma-Aldrich (St. Louis, MO, USA). Methanol, chloroform, and ethyl alcohol were obtained from Tianjin Chemical Reagent Company (Tianjin, China). *N*, *N*-(3-Dimethylaminopropyl)-*N*′-ethyl carbodiimide hydrochloride (EDC-HCl, 99% purity), *N*-hydroxysuccinimide (NHS) and L-ascorbic acid sodium salt (99% purity) were obtained from Alfa Aesar (Haverhill, MA, USA). Copper (II) sulfate pentahydrate ($CuSO_4{\cdot}5H_2O$, 98% purity) and all other chemical reagents, unless otherwise stated, were purchased from Tianjin Chemical Reagent Company. Biotin-conjugated anti-Sca-1 antibody (bs-3752R-Bio) was purchased from Bioss Biotechnology Co., Ltd. (Beijing, China). All cell culture reagents were purchased from Thermo Fisher Scientific (Waltham, MA, USA). Human platelet-rich plasma (PRP) was purchased from the Tianjin Blood Centre (Tianjin, China). Masson's Trichrome, Sirius Red and Safranin O staining kits were obtained from Leagene (Beijing, China), Haematoxylin and Eosin (H&E) and Verhoeff van Gieson (VVG) staining kits were obtained from Solarbio (Beijing, China). Primary antibodies (CD31, ab64543; α-SMA, ab7817; SM-MHC, ab683; CD68, ab125212; iNOS, ab15323; CD206, ab64693; vWF, ab6994; Collagen I, ab34710; and GFP, ab1218) were purchased from Abcam (Cambridge, UK). Primary antibodies (Collagen III, A0817; TNF-α, A11534; and IL-1β, A19635) were purchased from Abclonal (Wuhan, China). Primary Sca-1 antibody (AB4336) was obtained from Merck Millipore (Burlington, MA, USA). Primary RFP antibody (PA1-986) and all secondary antibodies were obtained from Invitrogen (Thermo Fisher Scientific). DiI and DIO dyes were purchased from Beyotime (Shanghai, China).

2.2. Preparation of electrospun PCL mats and vascular grafts

Firstly, PCL2K–N_3 was prepared using a two-step procedure as reported in previous studies [17,35]. Firstly, PCL2K-diol was reacted with p-toluenensulfonyl chloride (TsCl) to obtain PCL2K-TsO. Then, PCL2K-TsO and NaN_3 were mixed to initiate a nucleophilic substitution reaction that results in the formation of PCL2K–N_3. PCL scaffolds, including PCL fibrous mats and vascular grafts, were fabricated by electrospinning using a setup previously described [14]. Briefly, PCL80K was mixed with PCL2K–N_3 at blending ratio of 9:1 (w/w). The mixture was dissolved in mixed $CHCl_3$/MeOH (5:1, v/v) by sufficient stirring overnight to obtain homogeneous solution at 25% (w/v) concentration. Then, the polymer solution was fed continuously at a rate of 8 mL/h using a syringe pump through a 21G stainless-steel needle with an applied voltage (11 kV). The fibrous mats and vascular grafts were fabricated using a rotating stainless-steel mandrel (100 mm in diameter) and a stainless-steel rod collector (2 mm in diameter), respectively. The distance between the tip and the collector was 15 cm. As-prepared PCL mats and vascular grafts were placed into a vacuum for at least 72 h to remove residual solvent.

2.3. Biotin-avidin-antibody functionalization of PCL scaffolds

Functionalized PCL mats and vascular grafts were prepared using stepwise biotin-avidin conjugation (Fig. 1A), according to previous protocols [14]. First, biotin was immobilized onto the surface of the electrospun PCL scaffold through the click reaction between azide groups and alkynyl-biotin (Biotin-C≡CH, 2 mg/mL) in dimethyl formamide (DMF)/H_2O (1:2 vol) under the catalysis of $CuSO_4$/L-ascorbic acid sodium (1:10 M ratio) [36]. Next, the mixture was maintained at 37 °C for 24 h with gentle agitation. The resulting PCL-biotin scaffolds were rinsed with deionized water repeatedly and dried at room temperature. Avidin was then bound to the biotinylated PCL scaffolds with the aid of

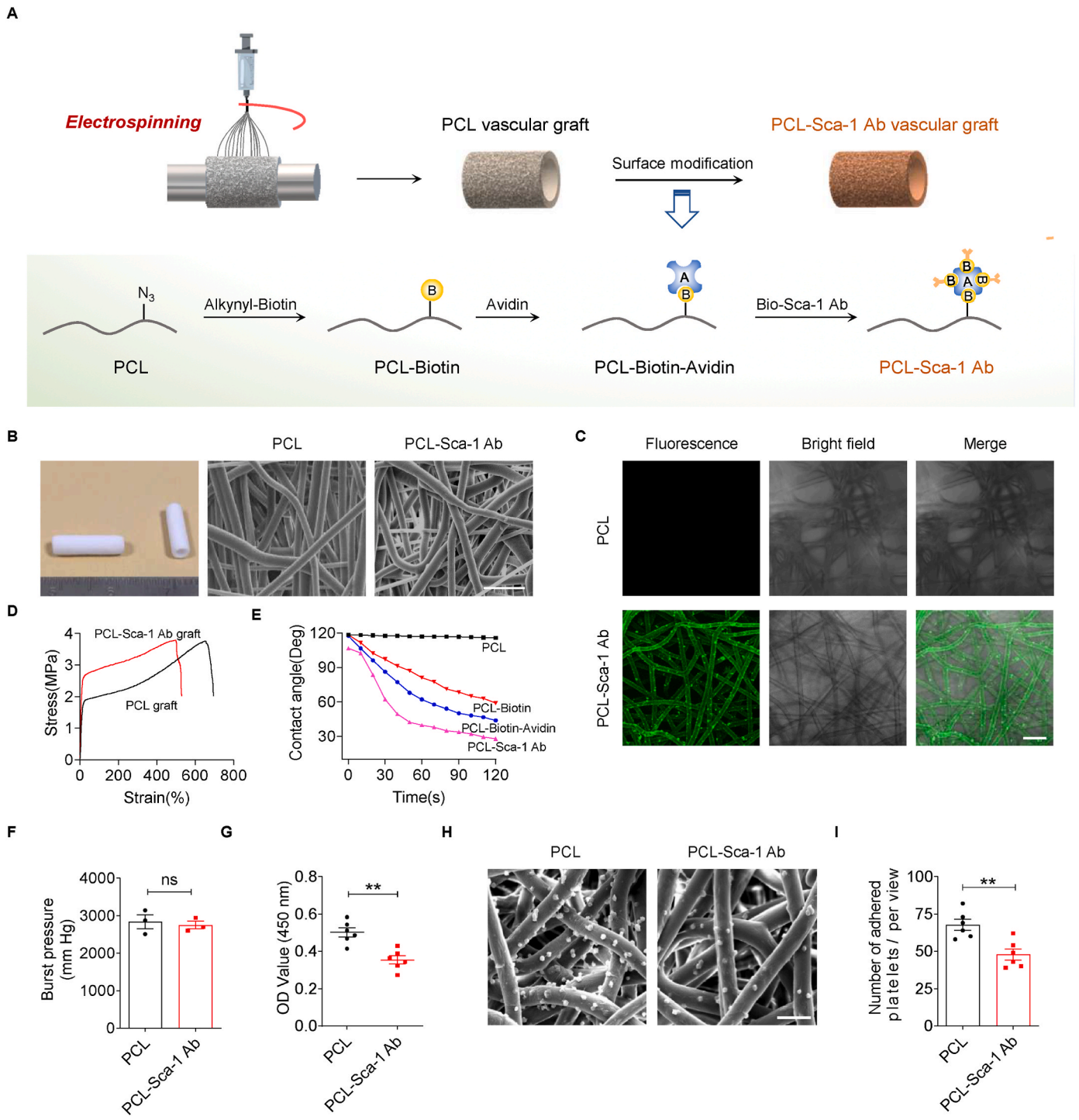

Fig. 1. Fabrication and characterization of anti-Sca-1 antibody-functionalized vascular grafts. (A) Experimental schematic for immobilization of anti-Sca-1 antibodies on electrospun PCL vascular graft. (B) Images show the tubular vascular grafts (1 cm in length) and representative SEM images of the electrospun PCL and PCL-Sca-1 Ab grafts. Scale bar for SEM images, 30 μm. (C) Representative confocal laser scanning microscopy (CLSM) images revealed that anti-Sca-1 antibodies were modified on electrospun PCL grafts. Scale bar, 20 μm. (D) Representative stress-strain curves of the PCL and PCL-Sca-1 Ab grafts. (E) Surface hydrophilic/hydrophobic performance characterized by static water contact angle measurement. (F) The burst pressure of the PCL and PCL-Sca-1 Ab grafts. Data were expressed as mean ± s.e.m. for each group, n = 3 independent experiments. (G) Quantitative analysis of the human plasma fibrinogen (FGN) adsorption on the different mats measured by ELISA. Data were expressed as mean ± s.e.m. for each group: $^{**}p < 0.01$. n = 6 independent experiments. (H) SEM images showed the platelet adhesion on the different mats. Scale bar, 10 μm. (I) Quantitative analysis of the adhered platelets. Data were expressed as mean ± s.e.m. for each group: $^{**}p < 0.01$. n = 6 independent experiments.

affinity interactions [37]. In detail, PCL-biotin scaffolds were submerged in avidin solution (0.5 mg/mL) and incubated at room temperature for at least 4 h. The resulting PCL-biotin-avidin scaffolds were washed with deionized water. Finally, PCL-biotin-avidin scaffolds were immersed in biotin-conjugated anti-Sca-1 antibody solution (10 μg/mL) and incubated at 4 °C overnight. The anti-Sca-1 antibody-functionalized PCL scaffolds (PCL-Sca-1 Ab) were washed thoroughly with deionized water to remove free antibodies, and then washed with PBS. In this study,

PCL/PCL-N_3 blended scaffolds, biotinylated PCL scaffolds, avidin-modified PCL scaffolds and biotin-conjugated anti-Sca-1 antibody-modified PCL scaffolds were denoted as PCL, PCL-biotin, PCL-biotin-avidin and PCL-Sca-1 Ab, respectively.

2.4. Characterization of functionalized scaffolds

The structure and morphology of PCL and PCL-Sca-1 Ab tubular grafts were analysed by scanning electron microscopy (SEM; FEI Quanta200, Prague, Czech Republic) with an accelerating voltage of 15 kV. The cross-section and inner surface of the tubular grafts were gold-sputter coated prior to SEM analysis. The outer and inner perimeters of the grafts were manually measured from SEM images of the cross-section with ImageJ software v1.41 (NIH, Bethesda, MD, USA) to determine the luminal diameter and wall thickness of the grafts (n = 6). Based on the SEM micrographs of the inner surface of grafts, the fiber diameter and pore size were analysed using ImageJ software. Porosity of the grafts was further determined using the liquid intrusion method, as previously described [14].

Surface chemistry was characterized using Fourier transform infrared spectroscopy (FTIR) at single attenuated total reflectance (ATR) mode (ATR-FTIR; Bio-Rad FTS 6000 spectrometer). The spectral resolution was 8 cm^{-1}. To evaluate the amount of immobilized avidin, we used [2-(4′-Hydroxy-azobenzene) benzoic acid] (HABA)/avidin reagent [38]. Briefly, HABA specifically binds avidin but with a lower binding affinity than biotin. The HABA/avidin complex has an absorption peak at around 500 nm. To determine the amount of avidin immobilized on PCL-Biotin grafts, avidin was first incubated with an excess of HABA to form fully saturated HABA/avidin complexes. Avidin/HABA absorbance was measured at 500 nm, before and after (30 min) addition of the PCL-Biotin. The change in absorbance is used to calculate the grafted avidin. A series of avidin solutions of varying concentration were prepared as a calibration curve for determining the quantity of avidin molecules present on the graft [39].

Immobilization of anti-Sca-1 antibodies was observed by confocal laser scanning microscopy (CLSM; Ziess LSM 710, Oberkochen, Germany). In detail, fluorescein isothiocyanate (FITC)-conjugated secondary antibodies were incubated with the PCL and PCL-Sca-1 Ab mats for 2 h at room temperature under darkness. Thereafter, PCL/FITC and PCL-Sca-1 Ab/FITC mats were rinsed at least 6 times with PBS to remove non-specific staining.

Mechanical properties of rectangular samples (6 × 20 × 0.50 mm; n = 3) taken from the tubular grafts were assessed using an Instron Universal Tensile Tester (Instron 5865, Norwood, MA, USA). The distance between two grips was set at 10 mm, and the tensile test was conducted at an ambient temperature, with a crosshead speed of 10 mm/min. The stress-strain curves were recorded, and the quantitative analysis of mechanical properties was calculated.

Surface wettability and water contact angles of the four types of prepared scaffold mats were measured using the Sessile drop method with a Harke-SPCA goniometer (Beijing, China). The mats were fixed on glass slides and placed onto the sample stage. The images were continuously recorded at room temperature.

The burst pressure of the graft was tested by a self-made machine and the protocol as described previously [19], burst pressure was measured by filling a graft segment (3 cm in length) with soft paraffin (Vaseline) whilst clamping one end and hermetically sealing the other with a catheter. A constant filling rate of 0.1 mL/min was applied, and the filling pressure was recorded until the graft wall burst.

2.5. Fibrinogen adsorption and platelet adhesion

The abundant plasma protein, fibrinogen (FGN), plays essential roles in thrombosis [40]. FGN adsorption onto PCL and PCL-Sca-1 Ab mats was assessed by enzyme-linked immunosorbent assay (ELISA). PCL and PCL-Sca-1 mats of appropriate size (~10 mm in diameter) were placed into 48-well plates and incubated with 30 μg/mL human FGN in PBS (200 μL/well) at 37 °C for 1 h to allow protein adsorption. After washing with PBS (3 min × 3), Human Fibrinogen ELISA Kits (UNOCI Biotechnology, Shanghai, China) were used according to the manufacturer's protocols and absorbance was measured at 450 nm using a microplate reader (iMark, Bio-Rad, Hercules, CA, USA).

Platelet adhesion assays were performed as reported previously [36]. In brief, PCL and PCL-Sca-1 mats of appropriate size were placed into 48-well plates and incubated with 300 μL platelet-rich plasma (PRP) per well at 37 °C for 1 h to allow platelet adhesion. The concentration of PRP was 1×10^8 platelets/mL. The unattached platelets were rinsed off with PBS three times. Mats were submersed in 2.5% glutaraldehyde (200 μL/well) overnight at 4 °C and rinsed with PBS three times. Finally, the mats were dehydrated with alcohol gradients (70%–100%, 5 min each) in sequence, and allowed to dry at room temperature. Adhered platelets were observed by SEM, following the same SEM methodology above. For the platelet adhesion measurements, each group had six replicate samples. Six different positions were selected for each sample for image capture, and the averaged values of the six images were used to determine the mean ± s.e.m. of the six samples for statistical analysis.

2.6. Sca-1^+ vascular stem/progenitor cells (Sca-1^+ SPCs) isolation, sorting and culture

Sca-1^+ SPCs were acquired from explanted aortic adventitial tissues, as previously described [29,41]. Briefly, the aortic arch and root from Sprague-Dawley (SD) rats were harvested under sterile conditions. The adventitia was carefully detached from the media and intima layers, cut into pieces, seeded onto gelatin-coated flasks, and cultured with Dulbecco's modified Eagle medium (DMEM; Thermo Fisher Scientific) supplemented with 20% ES Cell Qualified Foetal Bovine Serum (FBS; Thermo Fisher Scientific), 0.1 mM β-mercaptoethanol (Sigma-Aldrich), 10 ng/mL leukemia inhibitory factor (LIF; Merck Millipore) and 100 U/mL penicillin/streptomycin (GIBCO, Thermo Fisher Scientific). Cells were cultured in humidified incubators at 37 °C with an atmosphere of 5% CO_2. After outgrowth and flasks reached 90% confluency, Sca-1^+ cells were isolated with anti-Sca-1^+ immunomagnetic microbeads (Miltenyi Biotec, Cologne, Germany) and sorted with a magnetic cell separator following the manufacturer's instructions. The purity of the enriched primary cell cultures was assessed by flow cytometry [29]. Briefly, cells collected and washed with PBS and fixed with 4% paraformaldehyde. Then, cells were stained using polyclonal anti-Sca-1 (1:100) as primary antibody and FITC labeled goat anti-rabbit as second antibody. Flow cytometric assay was performed on a FACS Calibur (BD, USA), and data were analysed by FlowJo software (Tree Star, Ashland, Ore). The isolated cells were then cultured in stem cell complete medium (DMEM with 10% FBS, 10 ng/mL LIF, 0.1 mM β-mercaptoethanol, 100 U/mL penicillin/streptomycin).

2.7. In vitro analysis of targeted recruitment, capture, and retention of SPCs

The ability of anti-Sca-1 antibody-functionalized PCL mats to recruit Sca-1^+ SPCs was determined by cell attachment assays under static culture conditions. The PCL, PCL-Biotin, PCL-Biotin-Avidin, and PCL-Sca-1 Ab mats were placed into 48-well tissue culture polystyrene plates (TCPs; Costar, Corning, NY, USA) and sterilized by UV irradiation for 30 min. Two different cell trackers, DIO and DiI cell-labeling solutions (Beyotime), were used to label Sca-1^+ SPCs in either serum-free or serum-containing medium, respectively, according to the manufacturer's protocols. A total of 300 μL DIO-labeled SPCs (5×10^4 cells/mL) were seeded in each well in serum-free medium, and cultured under gentle shaking to avoid physical aggregation of cells. After 1 h, non-adherent cells were removed by washing with PBS. Adherent cells were fixed with 4% paraformaldehyde, washed with PBS (3 min × 5), and stained with 4,6-diamidino-2-phenylindole (DAPI)-containing

mounting solution (SouthernBiotech, Birmingham, AL, USA). The cells were visualized by CLSM, and the number of attached cells on the mats was counted. Specifically, each group has six replicate samples. Six randomly selected fields (× 200 view) were photographed for each sample, and the cell numbers per field were manually counted and the average for each sample was determined. The averaged values were used to the determine the mean ± s.e.m. of the six samples for statistical analysis.

A dynamic culture flow system bioreactor (TEB500, EBERS Medical Technology, Zaragoza, Spain) was utilized to evaluate the ability of anti-Sca-1 antibody-functionalized vascular grafts to capture Sca-1$^+$ SPCs under flow culture conditions. The bioreactor was designed as a closed-loop perfusion system (Fig. 2C); the bioreactor was a culture chamber that consisted of three parts: rubber tubing for medium recirculation, feeding, and outflow; a cell culture bottle containing stem cell culture medium; and a peristaltic pump to control perfusion flow speed. The PCL and PCL-Sca-1 Ab grafts (1 cm in length) were attached to the rubber tubing. Subsequently, the peristaltic pump with preassembled sterile rubber tubing was attached and the system was rinsed with PBS and serum-free stem cell medium before cell inoculation. DIO- labeled Sca-1$^+$ SPC suspensions (2 × 10^6 cells/mL) cultured in 30 mL serum-free or serum-containing medium in cell culture bottles were attached to begin perfusion. The recirculation was tested under 12 dyn/cm^2 shear stress. The bioreactor system was maintained in a humidified atmosphere of 5% CO_2 at 37 °C. After 2 h of recirculation, the PCL and PCL-Sca-1 Ab grafts were detached, snap-frozen in Tissue-Tek Optimal Cutting Temperature (OCT) compound (Sakura Finetek, Torrance, CA, USA), and cut into 6 μm thick cross-sections. The cell capturing properties of the PCL and the PCL-Sca-1 Ab grafts were assessed by staining the cross-sections with DAPI. Cross-section images were used to quantify the number of captured DIO-labeled SPCs. Specifically, each group had six replicate samples. Six cross-sections at different positions were taken from each sample, and the number of cells in each cross-section was counted and averaged to determine the sample value. Averaged values were used to calculate the mean ± s.e.m. of the six samples for statistical analysis.

Cell retainment assays were conducted to assess the retainment of

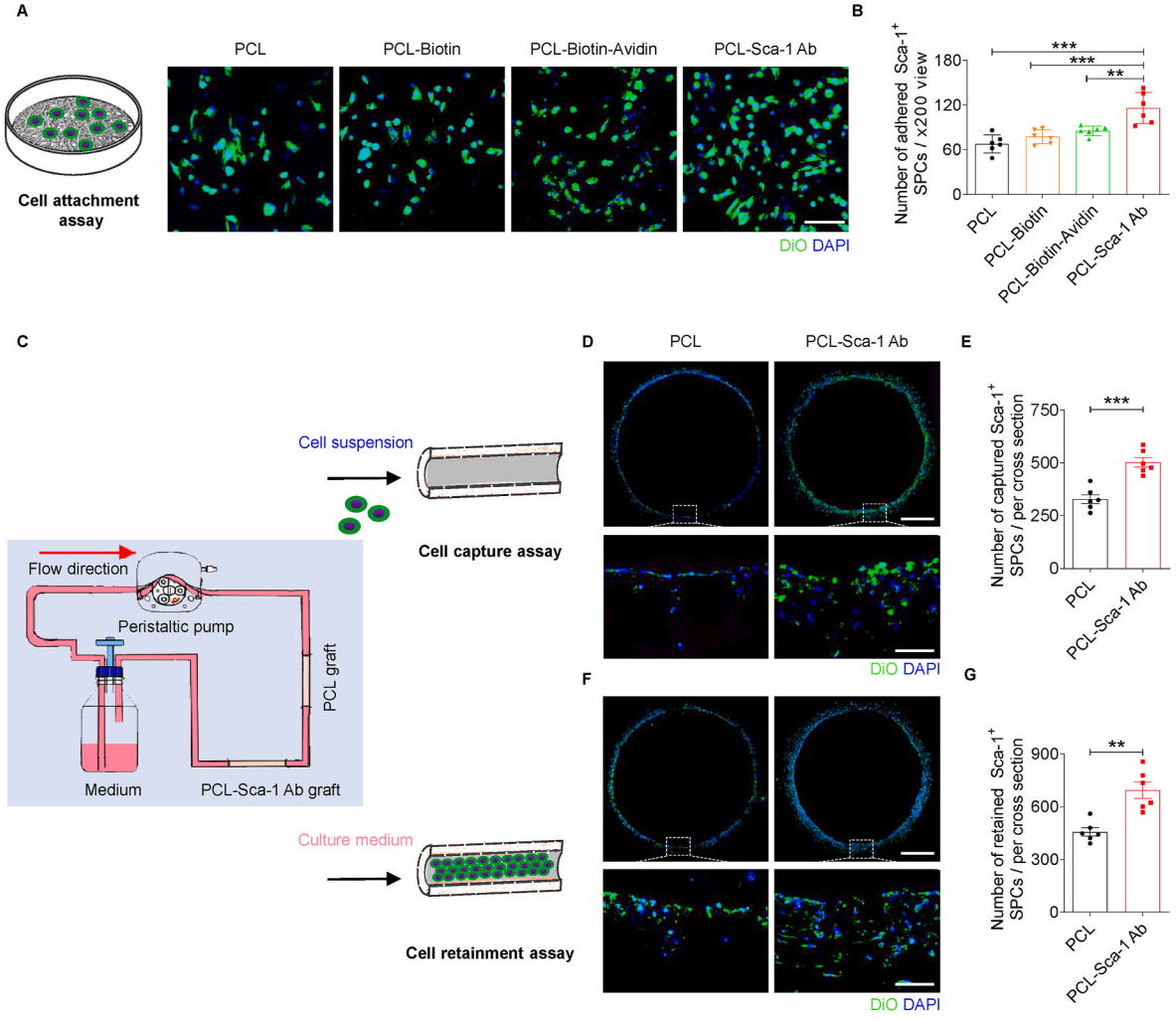

Fig. 2. Anti-Sca-1 antibody modification significantly enhances the recruitment, capture, and retainment of Sca-1$^+$ SPCs on PCL vascular grafts in serum-free medium *in vitro*. (A) Representative CLSM images of the DiO-labeled Sca-1$^+$ SPCs attached to different groups of PCL mats under static culture. Scale bar, 100 μm. (B) The number of attached Sca-1$^+$ SPCs was quantified. Data were expressed as mean ± s.e.m. for each group: $^{**}p < 0.01$, $^{***}p < 0.001$. n = 6 images per sample, with a total of 6 samples per group. (C) Schematic illustration of dynamic flow culture of cells *in vitro*. (D) Representative CLSM images of DiO-labeled Sca-1+ SPCs on the PCL and PCL-Sca-1 Ab grafts after dynamic capture (12 dyn/cm^2) for 2 h. Scale bars, 500 μm or 100 μm (magnified images). (E) Quantitative analysis of the number of captured Sca-1$^+$ SPCs on different grafts after dynamic flow culture. Data were expressed as mean ± s.e.m. for each group: $^{***}p < 0.001$. n = 6 images (different regions of the graft) per sample, with a total of 6 samples per group. (F) Representative CLSM images of the DiO-labeled Sca-1$^+$ SPCs retained on the PCL and PCL-Sca-1 Ab grafts after 6 h of dynamic flow culture (12 dyn/cm^2). Scale bars, 500 μm or 100 μm (magnified images). (G) Quantitative analysis of the number of retained Sca-1$^+$ SPCs on different grafts after dynamic flow culture. Data were expressed as mean ± s.e.m. for each group: $^{**}p < 0.01$. n = 6 images (different regions of the graft) per sample, with a total of 6 samples per group.

Sca-1$^+$ SPCs on anti-Sca-1 antibody-functionalized vascular grafts. PCL and PCL-Sca-1 Ab grafts (1 cm in length) were carefully preseeded with 200 μL DIO-labeled Sca-1$^+$ SPCs (1×10^7 cells/mL) by direct application to the graft lumens. The seeding process was repeated 5 times, and after each application, an interval of 2 min was used to rotate the vascular grafts to promote uniform distribution and to provide a homogeneous gravity environment. After 2 h of culture, grafts were rinsed with PBS to remove nonadherent cells before the grafts were attached to the bioreactor flow system. Then, 30 mL of stem cell culture medium was added to the cell culture bottle and used to perfuse the system. The recirculation was also tested under 12 dyn/cm^2 shear stress, which was more similar to the physiological condition. The bioreactor flow system was maintained under standard culture conditions and steady laminar shear stress was allowed to persist for 6 h before the grafts were harvested for analysis, and processed as described above.

Cell proliferation was evaluated by seeding Sca-1$^+$ SPCs (1×10^4 cells/well) into 48-well TCPs or TCPs containing PCL and PCL-Sca-1 Ab mats. One hour after seeding, nonadherent cells were removed by washing with PBS. The stem cell culture media was refreshed every 2 days. On days 1, 3, and 5, Cell Counting Kit-8 (CCK-8; Dojindo Laboratories, Kumamoto, Japan) was used to quantitatively assess the cell metabolic activity as related to cell numbers.

2.8. In vivo implantation in rats

Sprague-Dawley rats (SD rats, male, 280–320 g) were obtained from Vital River Laboratory Animal Technology (Beijing, China). All animal procedures were approved by the Centre of Tianjin Animal Experiment Ethics Committee and Authority for Animal Protection. The rat recipients of vascular grafts were randomly divided into 6 groups (PCL [3 days], [2 weeks] and [4 weeks]; PCL-Sca-1 Ab [3 days], [2 weeks] and [4 weeks]; n = 3/group for 3 days, and n = 6/group for 2 and 4 weeks). The rats were fasted for 24 h prior to surgery. Rats were anesthetized by intraperitoneal injection of chloral hydrate (300 mg/kg) before being placed under the operating microscope in a supine position, and limbs were affixed to the surgical table. Heparin (100 U/kg) was administered by tail vein injection before surgery. A midline laparotomy incision (4–5 cm) was made, and the abdominal aorta was isolated, clamped, and transected. The grafts (2 mm in lumen diameter, 1 cm in length) were anastomosed to the abdominal aorta and secured with an end-to-end fashion with 8–10 interrupted stitches using 9-0 monofilament nylon sutures (Ling Qiao, Ningbo, China). Finally, blood flow was restored, and the incision was closed with 3-0 nylon sutures. Rats were then placed into clean and dry cages on heating pads to maintain body temperature until the rats recovered from anaesthesia. The patency of the implanted vascular grafts was assessed at the indicated timepoints using high-resolution ultrasound (Vevo 2100, Visual Sonics, Toronto, Canada), following rat anesthetization with isoflurane gas.

2.9. Mouse model generation and bone marrow transplantation

C57BL/6 mice (male, 20–25 g) were purchased from Vital River Laboratory Animal Technology (Beijing, China). *Sca1 2A-CreER* mice (C57BL/6 background) and *Rosa-RFP* mice (C57BL/6 background) were kindly provided by Professor Bin Zhou (Shanghai Institute of Biochemistry and Cell Biology). *Sca1 2A-CreER; Rosa-RFP* lineage tracing mice were obtained by crossing *Sca1 2A-CreER* mice with *Rosa-RFP* mice. All male and female mice used in this study were aged 8 weeks at the time of experiments. The use of experimental animals was approved by the Animal Experiments Ethical Committee of Nankai University and carried out in conformity with the Guide for Care and Use of Laboratory Animals. Green fluorescence protein (*GFP*) transgenic mice (C57BL/6 background, male) were purchased from Shanghai Model Organisms Center.

We harvested bone marrow cells via collecting and flushing the cavities of femurs and tibias isolated from *GFP* transgenic donor mice, using 1–1.5 mL RPMI 1640 medium (BI, 01-100-1A). Bone marrow cells were then passed through 40 μm cell strainers (Falcon, 352340) to obtain single cell suspensions, followed by re-suspension in RPMI 1640 medium prior to transplantation. Eight-week-old male *Sca1 2A-CreER; Rosa-RFP* lineage tracing mice had undergone 4 Gy of sub-lethal whole-body irradiation split into two doses and separated by 4 h. Six hours later, they were transplanted with 5×10^6 bone marrow cells harvested from the femurs of age- and sex-matched *GFP* transgenic mice via tail vein injection to form chimeric mice. The chimeric mice were maintained in a specific pathogen-free environment and received normal chow and drinking water with enrofloxacin after bone marrow transplantation.

2.10. Graft implantation into bone marrow transplanted mice

Chimeric mice were generated as above. Briefly, bone marrow cells from *GFP* transgenic mice were transferred to irradiated *Sca1 2A-CreER; Rosa-RFP* lineage tracing mice and further pulsed with tamoxifen (20 mg/mL) 4 weeks later via intraperitoneal injection (100 mg/kg body weight) once a day for a time period of 3 days. Two weeks later, the chimeric mouse received graft implantation.

Aortic segments for implantation were harvested from C57BL/6 wild-type mice, washed and suspended in saline solution containing heparin (100 U/mL). Decellularization was performed by treating the aortic segments with 0.04% SDS (Sangon Biotech, China) in a shaker for 4 h at room temperature. Subsequently, they were washed thoroughly with saline at room temperature. The decellularized aortic segments were further modified by heparinization in PBS solution containing 1 mg/mL heparin, 5.751 mg/mL EDC, and 5.179 mg/mL NHS at 4 °C for 12 h, followed by washing with saline three times at 4 °C. The heparinized aortic segments were stored in 1% penicillin-streptomycin PBS solution at 4 °C. All steps were performed under sterile conditions.

Chimeric mice were anesthetized using a combination of Hypnorm (25 mg/kg; Veta Pharma, UK) and Hypnovel (25 mg/kg; Roche) administered intraperitoneally. The right common carotid artery was mobilized free from the bifurcation at the distal end toward the proximal end, cut in the middle, and a cuff was placed over the end. The cuff was made from an autoclavable nylon tube (0.63 mm in outer diameter, 0.5 mm in inner diameter) (Portex, Hythe-Kent, UK). The artery was turned inside-out over the cuff and ligated. The decellularized aortic grafts were anastomosed to the two ends of the carotid artery by sleeving the ends of the graft over the artery cuff and ligating them together with an 8-0 suture. Finally, the blood flow was restored, and the muscle and skin incisions were closed with 6-0 nylon sutures. Aspirin was administered daily as an anticoagulant for 1 week (2 mg/kg). The mice were kept in cages with food and water normally. The patency of the implanted vascular grafts was assessed at the indicated timepoints using high-resolution ultrasound (Vevo 2100, Visual Sonics, Toronto, Canada), following mouse anesthetization with isoflurane gas.

2.11. Histological analysis

At predetermined timepoints, rats and mice were sacrificed. The grafts were explanted, rinsed with saline to remove excess blood, and processed for histochemical analysis, as described in previous literature [42]. The graft explants were bisected; one half was observed by a stereoscopic microscope (Leica S8AP0, Wetzlar, Germany) and then embedded in OCT compound and snap-frozen in liquid nitrogen for cross-sectioning; the other half was longitudinally cut into two pieces. One of the longitudinally cut pieces was observed under stereomicroscopy before being snap-frozen in OCT for longitudinal sectioning. The other piece was further divided into two more pieces and prepared for SEM or *en face* immunofluorescence staining.

Briefly, the samples for SEM were fixed with 2.5% glutaraldehyde overnight, dehydrated using an ethyl alcohol gradient (70%–100% series) for 5 min each, and then air-dried at room temperature. Samples

were mounted onto aluminum stubs, sputter-coated with gold, and visualized by SEM. For *en face* immunofluorescence staining, the samples were fixed with 4% paraformaldehyde solution for 30 min and then incubated with 5% normal goat serum (Zhongshan Golden Bridge Biotechnology, China) for another 30 min at room temperature. Next, the samples were incubated with CD31 (1:100) and Sca-1 primary antibodies in 0.01 mM PBS overnight at 4 °C, followed by incubation with secondary antibody in PBS for 2 h at room temperature. Finally, the samples were counterstained with DAPI and visualized with CLSM.

For histological analysis, the samples embedded in OCT were cut into 6 μm thick sections that were stained with H&E, Safranin O, Masson's Trichrome, VVG or Sirius Red stains, according to standard laboratory protocols. Mounted samples were observed under a bright field microscope (Leica DM3000), and staining was quantified by ImageJ software. For immunofluorescent staining, frozen sections were fixed in ice-cold acetone for 10 min, air-dried, and then rinsed with PBS (5 min × 2). Slides were then incubated in 5% normal goat serum for 45 min at room temperature. For intracellular antigen staining, 0.1% Triton X-100-PBS was used to permeate the cell membranes before blocking with serum. Slides were incubated with primary antibodies in PBS overnight at 4 °C, followed by PBS washes (5 min × 6) and incubation with secondary antibody in PBS for 2 h at room temperature. The nuclei were counterstained with DAPI-containing mounting solution. EC staining was performed using monoclonal mouse anti-CD31 (1:100) or anti-von Willebrand factor (vWF; 1:200) primary antibodies. Endothelial coverage rate was calculated according to the following equation: Endothelial coverage (%) = Length of CD31-labeled endothelium (μm)/ Total length of longitudinal graft section (μm) × 100. The smooth muscle cells were stained using rabbit anti-α-SMA (1:100) and mouse anti-smooth muscle myosin heavy chain I (SM-MHC; 1:100) primary antibodies. Collagen deposition was determined by immunofluorescence staining using rabbit anti-collagen I (1:100) and rabbit anti-collagen III (1:100) primary antibodies. To assess Sca-1$^+$ SPC recruitment, sections were stained with anti-Sca-1/Ly6A/E antibody (Sca-1; Merck Millipore, 1:100) overnight at 4 °C. To further investigate the source of Sca-1$^+$ SPCs, the sections were further stained with anti-GFP (1:1000) and anti-RFP primary antibodies (Invitrogen, 1:200), respectively. To detect macrophage infiltration, sections were incubated with anti-CD68 antibody (1:100). Furthermore, the classically activated (M1) and alternatively activated (M2) macrophages were stained using anti-iNOS (1:100) and anti-CD206 (1:100) primary antibodies, respectively. Inflammatory factors were visualized by immunofluorescence staining using anti-IL-1β (1:100) and anti-TNF-α (1:100) primary antibodies, respectively. Alexa Fluor 488 goat anti-mouse IgG (1:200, Invitrogen) and Alexa Fluor 594 goat anti-rabbit IgG (1:200, Invitrogen) were used as the secondary antibodies, as appropriate. Sections without primary antibody incubation were used as negative controls and discounted background staining/autofluorescence. Images were observed under a fluorescence microscope (Zeiss Axio Imager Z1) and staining was quantified by ImageJ software.

2.12. Statistical analysis

All quantitative results were obtained from at least three samples for analysis. GraphPad Prism Software v8.02 (San Diego, CA, USA) was used for statistical analysis. Student's *t* tests were used for comparisons of means between two groups. Multiple comparisons were performed using one-way analysis of variance (ANOVA) followed by Tukey's multiple comparisons test or two-way ANOVA followed by Sidak's multiple comparison test. $p < 0.05$ was considered statistically significant.

3. Results

3.1. Fabrication and characterization of anti-Sca-1 antibody-functionalized vascular grafts

The PCL grafts (2 mm in inner diameter) were successfully prepared by electrospinning. PCL is a linear aliphatic polyester without side chains or end groups. Thus, low molecular weight PCL with ends capped with azide groups (PCL2K–N_3) was introduced and blended with PCL80K (w/w, 1:9) to add a high density of azide reaction sites for later click chemistry addition of alkynyl-biotin for further surface functionalization [17,43,44]. After alkynyl-biotin reacted with the azide-rich PCL microfibers, avidin was immobilized by high affinity binding to biotin. Avidin provided active sites for the binding of biotin-conjugated anti-Sca-1 antibodies. A mild functionalization procedure was utilized to preserve the binding activity of the anti-Sca-1 antibodies (Fig. 1A).

SEM images (Fig. 1B) demonstrated that the electrospun PCL-Sca-1 Ab grafts had a well-defined microfibrous structure with an average fiber diameter of 7.5 ± 0.4 μm and pore size of 17.9 ± 1.3 μm. The cross-sections (Fig. S1) of the tubular grafts demonstrated homogeneous fiber distribution, and the microfiber morphology and porosity of the PCL grafts after anti-Sca-1 Ab modification remained unaltered. The statistical analysis showed that the luminal diameters were 1956 ± 41 μm for PCL grafts and 1964 ± 38 μm for PCL-Sca-1 Ab grafts, and the wall thickness that we prepared were 542.2 ± 33.8 μm for PCL grafts and 522.1 ± 22.6 μm for PCL-Sca-1 Ab grafts (Table S1).

The surface chemistry of functionalized PCL surface was characterized by ATR-FTIR. An evident peak at 2096 cm^{-1} displayed on the PCL spectrum, which is attributed to the stretching of azide group from the PCL2K–N_3. After the click reaction with alkynyl-biotin, this peak disappeared, indicating the substitution of azide groups. Peaks at 1550 cm^{-1} were detected in both the spectra obtained from PCL-Biotin and PCL-Biotin-Avidin, corresponding to the amide groups (Fig. S2). The avidin immobilized on the graft was quantified using the [2-(4′-Hydroxy-azobenzene)benzoic acid] (HABA)/avidin reagent, and was quantitatively equivalent to 0.1429 mg per graft (1 cm in length).

Immunofluorescent staining verified that the anti-Sca-1 antibodies were successfully immobilized on the graft microfibers in a homogeneous distribution (Fig. 1C).

The mechanical properties of the PCL grafts before and after antibody modification were evaluated by tensile testing (Fig. 1D). Mechanical properties, including maximum stress, strain-at-break, and Young's modulus were recorded (Table S2). The stress-strain curve of PCL-Sca-1 Ab grafts was similar to that of PCL grafts (max stress PCL 3.74 ± 0.42 MPa *versus* PCL-Sca-1Ab 3.78 ± 0.37 MPa). There was a decrease in tensile strength (elongation at break PCL 723.8 ± 15.9% *versus* PCL-Sca-1 Ab 550.5 ± 21.5%) and a slightly increased Young's modulus (PCL 13.37 ± 0.84 MPa *versus* PCL-Sca-1 Ab 17.53 ± 0.68 MPa) following anti-Sca-1 antibody modification, but the grafts retained sufficient mechanical strength deemed appropriate for application as arterial vascular grafts [45].

The hydrophilicity/hydrophobicity of the graft surface is a major determinant of cell adhesion and survival [46,47]. Hydrophobic PCL mats showed a large water contact angle (115.6°, 120 s). After surface functionalization with biotin, the water contact angle of the mats significantly decreased to approximately 58.9°. Hydrophobicity was further changed when anti-Sca-1 antibodies were immobilized onto the mats; the water contact angle was reduced to 27.8° (Fig. 1E). In short, surface functionalization moderately lowered the PCL mat's hydrophobicity property, which is suggested to be more favourable for cell adhesion [46].

The assessed burst pressure of the PCL and PCL-Sca-1 Ab grafts showed that there were no significant differences between the PCL and PCL-Sca-1 Ab grafts (Fig. 1F). Both grafts demonstrated burst pressure values above the 1600 mmHg threshold required for withstanding arterial pressure [6].

3.2. Hemocompatibility of anti-Sca-1 antibody-functionalized vascular grafts

The plasma protein, fibrinogen (FGN), plays important roles in platelet activation and mediation of platelet adhesion. FGN adsorption was determined by ELISA assay. The results showed that the PCL mats had higher levels of FGN adsorption (Fig. 1G), and PCL-Sca-1 Ab mats had significantly decreased levels of FGN adsorption ($p < 0.01$), which likely resulted from low interfacial free energy with water after the multilayer functionalization procedure.

Platelet adhesion to materials has been generally recognized as an index for evaluating the hemocompatibility of blood-interfacing devices. The morphology of adherent platelets also reflects their activated state [48]. The number of platelets adhered to PCL and PCL-Sca-1 Ab mats was quantified based on the SEM images. The correlative statistical analysis showed that PCL-Sca-1 Ab had significantly less adhered platelets, compared to PCL ($p < 0.01$). Furthermore, most of the platelets adhered to the PCL-Sca-1 Ab mats were in an inactivated (round) state, and fewer were in an activated (dendritic) state, similar to the platelets adhered to the PCL fibers (Fig. 1H and I).

3.3. Assessment of recruitment, capture, and retainment of Sca-1$^+$ SPCs by anti-Sca-1 antibody-functionalized vascular grafts

The purity of the enriched primary Sca-1$^+$ cell cultures was assessed by flow cytometry. A majority of the cells expressed Sca-1$^+$, suggestive of a culture purity over 95% (Fig. S3). The isolated Sca-1$^+$ SPCs were used for subsequent *in vitro* experiments.

The attachment of Sca-1$^+$ SPCs to PCL and modified PCL mats was assessed *in vitro*. Cell adhesion is influenced by substrate surface hydrophobicity. As seen from the CLSM images, the number of Sca-1$^+$ SPCs that adhered to the PCL was the least amongst the groups. After functionalization, Sca-1$^+$ SPC attachment to PCL-Biotin and PCL-Biotin-Avidin mats tended to be improved, which was likely due to the ameliorative surface hydrophobicity, but the increase in cell attachment was not statistically significant compared to unmodified PCL. Therefore, this suggested that the extent of Sca-1$^+$ SPC adhesion could not be substantially improved by solely adjusting the PCL surface hydrophilicity/hydrophobicity. The number of adhered Sca-1$^+$ SPCs was significantly increased in the PCL-Sca-1 Ab group, compared to all other groups (Fig. 2A and B). The major reason for enhanced attachment can be ascribed to the immobilized anti-Sca-1 antibodies recognizing and strongly binding to cell-surface Sca-1 protein, which conveyed the improved recruitment and SPC adhesion by PCL-Sca-1 Ab mats.

To mimic the capture of SPCs *in vivo*, we next sought to determine whether anti-Sca-1 antibody-functionalized PCL grafts could capture DIO-labeled Sca-1$^+$ SPCs from a dynamic flow *in vitro* culture system (Fig. 2C). Cell capture assays were qualitatively and quantitatively analysed based on the DAPI-stained sections. The images of the graft cross-sections revealed that Sca-1$^+$ SPCs were successfully captured by PCL-Sca-1 Ab grafts. In contrast, the Sca-1$^+$ SPCs present on the PCL graft were mostly distributed at the bottom of the graft circumference, suggesting a contributory effect of gravity and cell rolling on material attachment (Fig. 2D). The number of Sca-1$^+$ SPCs was determined quantitively and supported the observations made by fluorescence microscope (Fig. 2E); there was robust Sca-1$^+$ SPC attachment on PCL-Sca-1 Ab grafts even under dynamic flow culture conditions.

Next, we sought to determine the capability of the grafts to retain cells under dynamic flow conditions. Sca-1$^+$ SPCs were seeded onto the lumens of PCL and PCL-Sca-1 Ab grafts, and allowed to adhere for 2 h. The seeded grafts were attached to the dynamic flow culture system and exposed under 12 dyn/cm^2 shear stress. Cell retention was quantified after 6 h under steady laminar shear stress. The DIO-labeled Sca-1$^+$ SPCs displayed evident colonization on PCL-Sca-1 Ab grafts in contrast to the PCL grafts, which verified that the Sca-1$^+$ SPCs were stably adherent on PCL-Sca-1 Ab grafts under dynamic flow culture. Fluorescent images of cross-sections demonstrated that Sca-1$^+$ SPCs still covered the entirety of the graft circumference in PCL-Sca-1 Ab grafts (Fig. 2F). Meanwhile, statistical analysis showed that a significantly larger number of Sca-1$^+$ SPCs were retained on PCL-Sca-1 Ab grafts compared to PCL grafts (Fig. 2G).

The proliferation rates of Sca-1$^+$ SPCs attached to the anti-Sca-1 antibody-functionalized vascular grafts were assessed (Fig. S4). On days 3 and 5, cell viability on the PCL-Sca-1 Ab mats was significantly improved compared to that on the PCL mats ($p < 0.01$). The results indicated that Sca-1$^+$ SPCs could grow on both mats, and that growth supported by PCL-Sca-1 Ab mats was enhanced over TCPs across the 5-day evaluation period. Thus, anti-Sca-1 antibody showed no inhibitory effect on Sca-1$^+$ SPC proliferation. Additionally, we evaluated the Sca-1$^+$ SPC binding capabilities of anti-Sca-1 antibody-functionalized grafts in the presence of serum. Our data showed that cell recruitment, capture and retainment remained unaffected by the presence of the supplemented soluble proteins (Fig. S5).

3.4. In vivo implantation and performance of anti-Sca-1 antibody-functionalized vascular grafts

The PCL and PCL-Sca-1 Ab vascular grafts were evaluated *in vivo* by implantation in rat abdominal aorta replacement models (Fig. 3A). The patency of the implanted grafts was examined by Doppler ultrasound after implantation (Fig. 3B). All grafts exhibited good patency without aneurysmal dilatation, bleeding, or material deformation. Further analysis by stereomicroscopy revealed that the luminal surfaces of both groups were smooth, clean, and free of macroscopic thrombi (Fig. 3C).

A 3-day rat abdominal aorta replacement model of acute inflammation was initially used to evaluate graft induction of the foreign body response through characterizing acute inflammatory reaction *in vivo*. Immunostaining for M1 macrophage (iNOS) phenotypes, IL-1β, and TNF-α were used to assess the macrophage response and pro-inflammatory factor production (Fig. S6A). The results revealed that PCL-Sca-1 Ab grafts produced levels of iNOS$^+$ M1 macrophages, IL-1β, and TNF-α that showed no differences compared to PCL grafts (Fig. S6B). Importantly, no acute inflammatory reaction at early stage (3-day) was observed after modification of anti-Sca-1 antibodies in the animal model *in vivo*.

Vascular tissue regeneration was analysed by H&E staining. Both graft groups showed good cellularization and neo-tissue formation. In the PCL-Sca-1 Ab graft group, a layer of well-organized neo-tissue was present on the lumen at 2 weeks, and this layer had been thickened by 4 weeks post-implantation. In contrast, the neo-tissue formed in PCL grafts were slightly increased in thickness between 2- and 4- weeks post-implantation (Fig. 3D). Moreover, there was no incidence of intimal hyperplasia, which was reflected by the absence of significant difference in luminal diameter size in both graft groups (Fig. 3E).

ECM remodelling is vital for vascular regeneration. ECM deposition was assessed by visualizing glycosaminoglycans (GAG) by Safranin O, collagen by Masson's Trichrome and Sirius Red staining, type I and III collagens by immunofluorescence staining, and elastin fibers by VVG staining. The histological and immunofluorescence images showed increases in all assessed ECM components between 2- and 4- weeks post-implantation in both graft groups. However, there were noticeably thicker GAG, collagen, and elastin fibers arranged within the neo-tissue layer in the PCL-Sca-1 Ab grafts at 4 weeks than in neo-tissue of the PCL grafts at 4 weeks (Figs. 3F and S7).

3.5. Enhanced endothelialization by anti-Sca-1 antibody-functionalized vascular grafts

The vascular endothelium provides a functional anti-coagulation barrier to prevent thrombosis and restenosis, and is essential for maintaining the *in situ* patency of artificial vascular grafts after implantation. The lumens of the implanted grafts were observed to assess endothelial

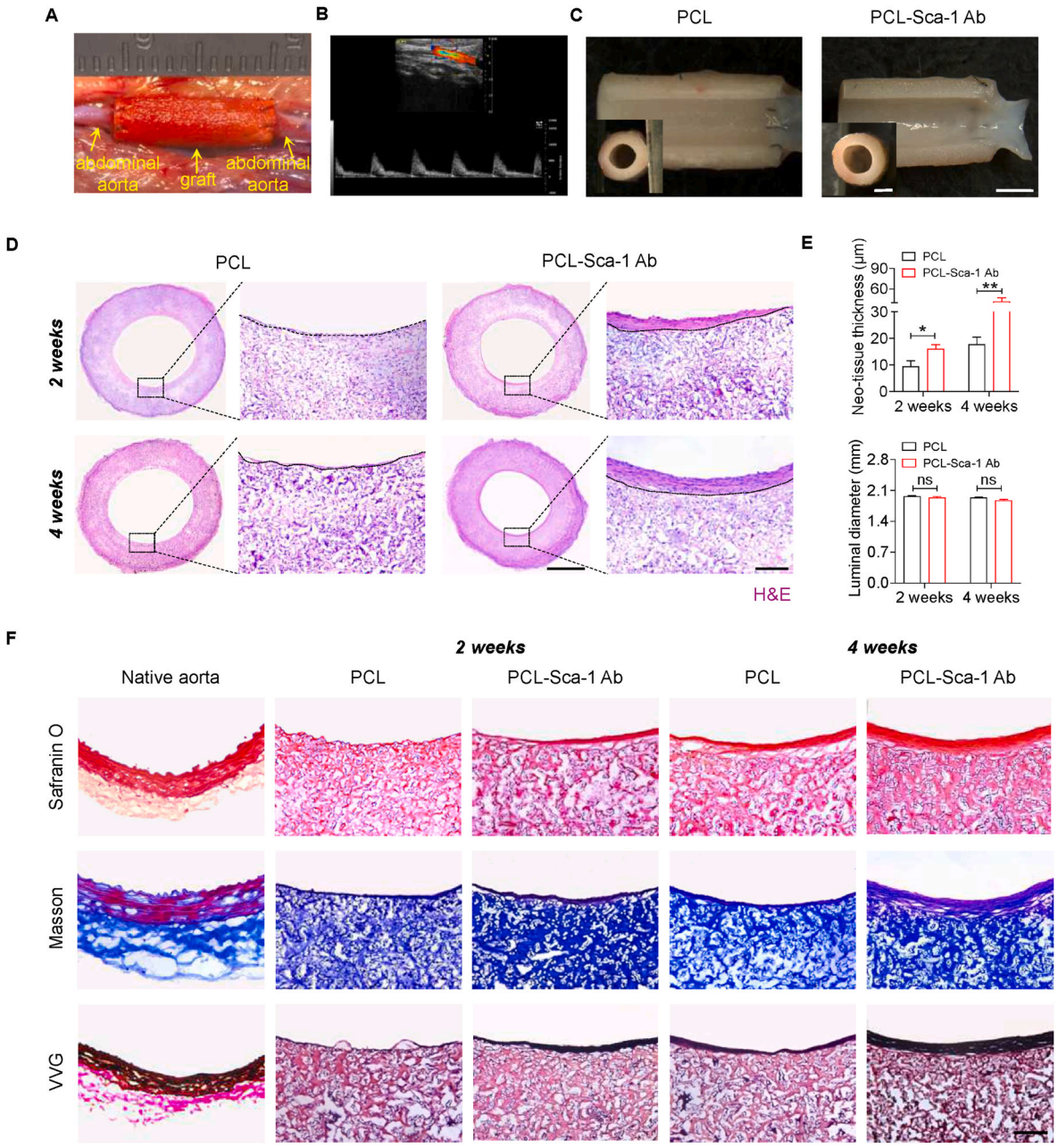

Fig. 3. Anti-Sca-1 antibody modification improves vascular regeneration *in vivo*. (A) Graft implantation in rat abdominal aorta replacement models. (B) Representative Doppler ultrasound image of the implanted PCL-Sca-1 Ab vascular graft. (C) Representative stereoscopic images of vascular grafts at 4 weeks post-implantation. Scale bars, 2 mm or 1 mm (inner panel). (D) Tissue regeneration within vascular grafts was analysed by H&E staining. The neo-tissue was bordered by dashed lines. Images are representative of n = 6 independent experiments. Scale bars, 1 mm or 100 μm (magnified images). (E) The average thickness of neo-tissue and the luminal diameter of implanted grafts were calculated based on the cross-sections with H&E staining. Data were expressed as mean ± s.e.m. for each group: $^{*}p < 0.05$, $^{**}p < 0.01$. (F) ECM reconstruction of implanted grafts was identified by Safranin O, Masson's Trichrome and Verhoeff-Van Gieson (VVG) staining to investigate the deposition of glycosaminoglycan, collagen and elastic fibers, respectively. Scale bar, 100 μm. Images are representative of n = 6 independent experiments.

cell (EC) coverage at three different positions, the anastomotic, quarter, and midportion sites. A discontinuous endothelium was observed in the quarter and middle sites in the PCL-Sca-1 Ab grafts at 2 weeks post-implantation (Figs. S8A and S8B). However, for PCL grafts, only anastomotic sites were populated by ECs, and the quarter sites were partially populated. The middle sites of PCL grafts had bare fibers at 2 weeks (Fig. S8A). SEM images (Fig. 4A) and *en face* immunostaining with CD31 antibody (Fig. 4B) performed at 4 weeks post-implantation demonstrated that ECs displayed a cobblestone-like morphology and were oriented in the direction of blood flow in the PCL-Sca-1 Ab groups, whereas there remained exposed fibers and CD31-negative cells were evident in the quarter and midportions of PCL grafts. Moreover, endothelial coverage and morphology in the PCL-Sca-1 Ab groups resembled those of the native artery. Immunofluorescence staining with anti-CD31 antibody in longitudinal sections showed a confluent monolayer of neo-endothelium covering all observed sections of the implanted PCL-Sca-1 Ab grafts at 4 weeks (Fig. 4C), whereas a partially formed neo-endothelium was present at the quarter site, and absent at the midportion of PCL grafts. Statistical analysis showed that the ratio of endothelial coverage of PCL-Sca-1 Ab grafts was significantly ($p < 0.01$)

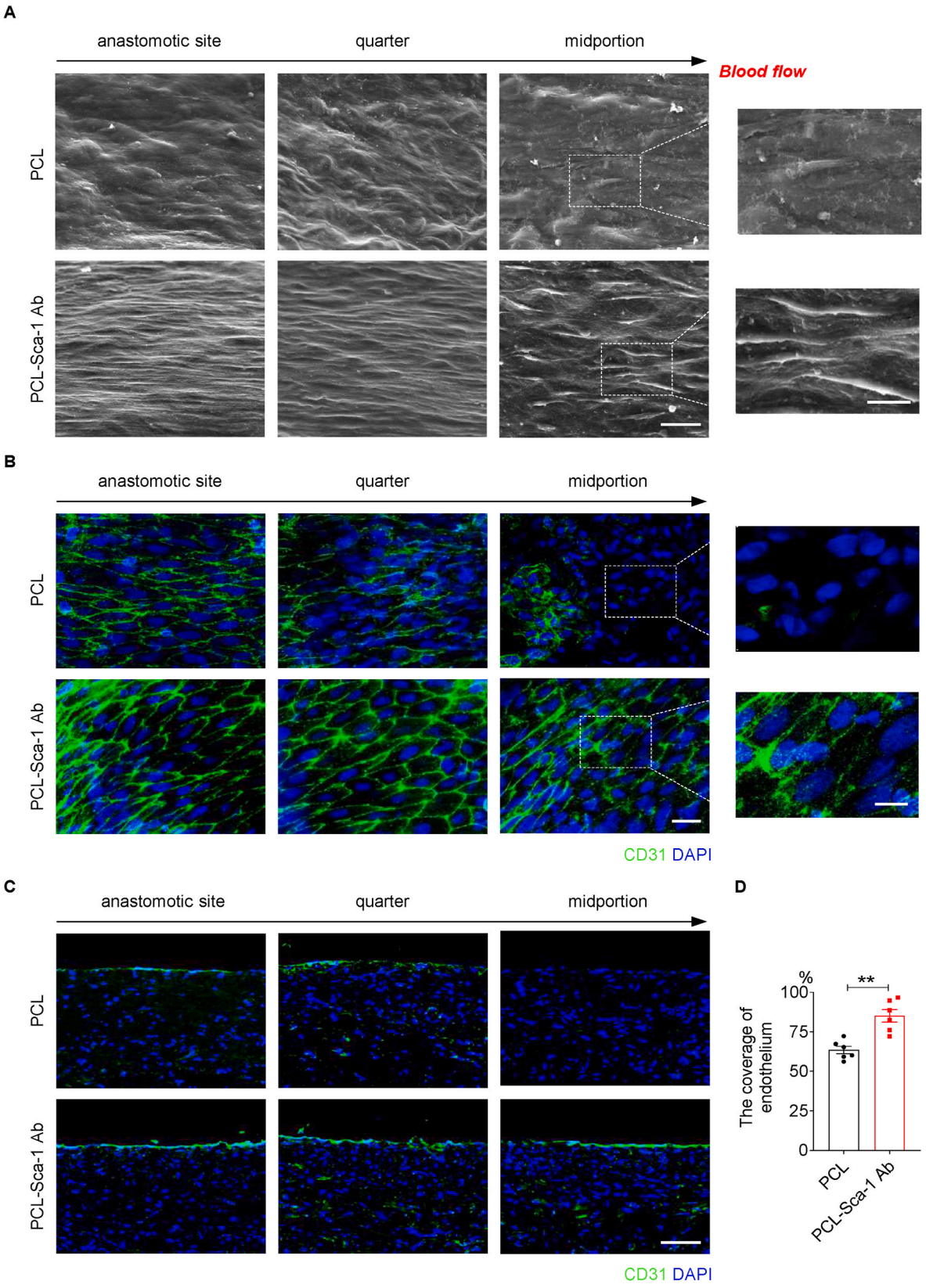

Fig. 4. Anti-Sca-1 antibody modification promotes the endothelialization at 4 weeks post-implantation *in vivo*. (A) SEM and (B) *en face* immunostaining images showed the endothelium distribution and morphology at different (anastomotic, quarter, and midportion) sites of the lumen. The direction of blood flow is indicated by the black arrow above each panel. Images are representative of n = 6 independent experiments. Scale bars for SEM images, 20 μm or 10 μm (magnified images). Scale bars for *en face* immunostaining images, 50 μm or 20 μm (magnified images). (C) Immunofluorescence staining with anti-CD31 antibody was performed to assess the endothelialization on longitudinal sections of the implanted grafts, and (D) the corresponding endothelium coverage rate was calculated. Nuclei were counterstained with DAPI. Scale bar, 100 μm. Data were expressed as mean ± s.e.m. for each group: $^{**}p < 0.01$. Images and data are representative of n = 6 independent experiments.

greater than that of the PCL grafts at 4 weeks (Fig. 4D).

3.6. Enhanced smooth muscle regeneration by anti-Sca-1 antibody-functionalized vascular grafts

Smooth muscle cells (SMCs) and their synthesized ECM provide the main structural stability of the vessel wall, and are imperative to the regulation of vascular tone in maintaining intravascular pressure and tissue perfusion functions. The regeneration of synthetic and contractile phenotype SMCs was evaluated by staining with α-SMA and SM-MHC antibodies, respectively. The fluorescence images of α-SMA$^+$ (Fig. 5A) showed that a layer of uniformly distributed α-SMA$^+$ cells was identifiable in the PCL-Sca-1 Ab groups at 2 weeks, and this became more densely arranged by 4 weeks (Fig. 5B). In the PCL graft groups, there was limited restoration of an α-SMA$^+$ cell layer at 2 weeks, and a significantly thinner layer had formed by 4 weeks. Meanwhile, SM-MHC exhibited a similar trend in both the PCL-Sca-1 Ab and PCL graft groups (Fig. 5C). The total thickness of the SM-MHC$^+$ neo-tissue layer showed a significantly greater thickness in PCL-Sca-1 Ab grafts, compared to the PCL grafts at 2- and 4- weeks post-implantation (Fig. 5D).

The organization and interface between EC and SMC layers were observed by double immunofluorescence staining with vWF (red, ECs) and α-SMA (green, SMCs) antibodies. The results revealed that ECs had formed a monolayer, while several layers of densely packed SMCs were arranged immediately below the neo-endothelium in PCL-Sca-1 Ab grafts at 4 weeks post-implantation. At 4 weeks in PCL grafts, a partial vWF$^+$ endothelial layer had formed, and this was above a thin α-SMA$^+$ layer; a large amount of α-SMA$^+$ cells remained within the graft walls, distal from the neo-tissue (Fig. 5E).

3.7. Infiltrated Sca-1$^+$ SPC contribution to regeneration orchestrated by anti-Sca-1 antibody-functionalized vascular grafts

In light of our *in vitro* experiments that demonstrated anti-Sca-1 Ab-functionalized vascular grafts increased Sca-1$^+$ SPCs recruitment and

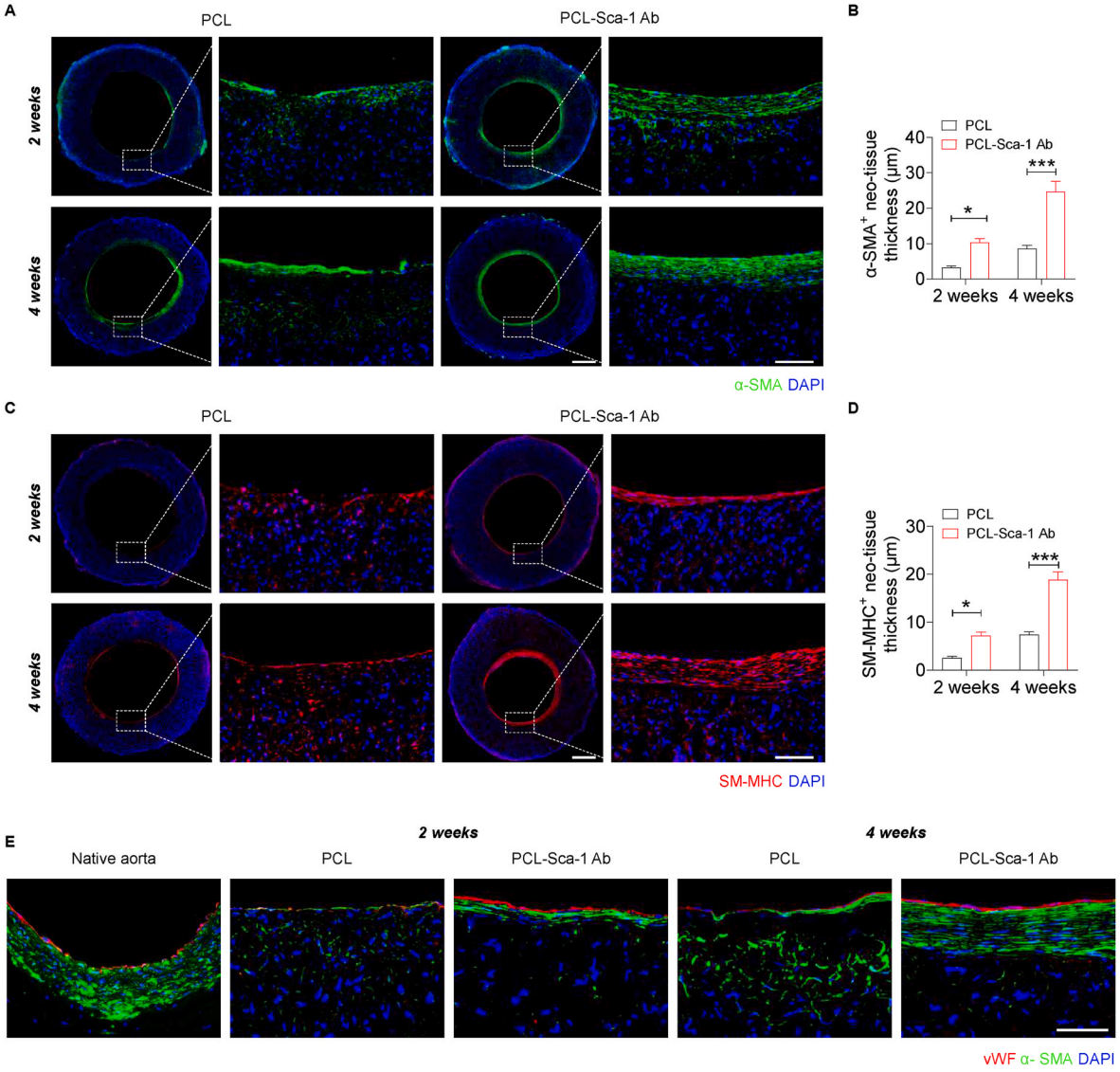

Fig. 5. Anti-Sca-1 antibody modification improves vascular smooth muscle regeneration, and enhances EC-SMC layer formation at 2- and 4- weeks post-implantation. (A) (C) Representative immunofluorescence images of PCL and PCL-Sca-1 Ab grafts showed SMC regeneration by staining the sections with anti-α-SMA and anti-SM-MHC antibodies, respectively. Scale bars, 500 μm or 100 μm (magnified images). (B) (D) Quantification of the average layer thickness of α-SMA and SM-MHC positive cells. Data were expressed as mean ± s.e.m. for each group: $^*p < 0.05$, $^{***}p < 0.001$. (E) The interaction between ECs and SMCs was observed by double immunofluorescence staining with anti-α-SMA and anti-vWF antibodies. Nuclei were counterstained with DAPI. Scale bar, 50 μm. Images and data are representative of n = 6 independent experiments.

capture, the *in vivo* recruitment and capture of Sca-1$^+$ SPCs was further investigated in rat abdominal aorta replacement models. Immunofluorescence staining for Sca-1$^+$ cells (Fig. 6A) indicated that PCL-Sca-1 Ab grafts remarkably enhanced the number of Sca-1$^+$ SPCs that had infiltrated the grafts, and their presence was detected at 2- and 4- weeks post-implantation. Quantitatively, the number of Sca-1$^+$ SPCs, as well as the ratio of Sca-1$^+$ SPCs in total cells within the vascular graft wall were all significantly ($p < 0.05$, or 0.001) increased in PCL-Sca-1 Ab grafts compared to PCL group due to anti-Sca-1 Ab modification (Fig. 6B and C).

Sca-1$^+$ SPCs are vital sources for tissue repair, regeneration, vascular homeostasis, and cell contribution to EC and SMC lineages under different stimuli. Co-immunostaining for CD31 (green) and Sca-1 (red) was used to investigate the infiltration and differentiation of recruited/captured Sca-1$^+$ SPCs to ECs *in vivo*. The results showed that there were CD31$^+$ Sca-1$^+$ cells detectable on the PCL-Sca-1 Ab grafts, indicating that these regenerated ECs were partially derived from the Sca-1$^+$ SPCs, and their coverage was more affluent than in the PCL grafts (Figs. 6D and S9). However, the ratio of CD31$^+$ Sca-1$^+$ cells/Sca-1$^+$ SPCs was similar between the two groups (Fig. 6E). These data suggested that antibody modification had a greater effect on the recruitment/capture of Sca-1$^+$ SPCs to the graft, but Sca-1$^+$ SPCs demonstrated a robust differentiation towards endothelial lineages regardless of graft modification.

Previous study has proved that Sca-1$^+$ SPCs autonomously and preferentially commit to an SMC fate. Sca-1$^+$ SPC differentiation into SMCs was confirmed by *in vitro* experiments (Fig. S10). Sca-1$^+$ SPCs were seeded on 24-well plates, cultured in the absence of LIF under static culture conditions for 1–3 days and autonomously differentiated into SMCs. To assess whether recruited/captured Sca-1$^+$ SPCs contributed to SMC regeneration, co-immunostaining with α-SMA (green) and Sca-1 (red) antibodies was performed (Fig. 6F). The results demonstrated that a proportion of α-SMA$^+$ Sca-1$^+$ cells were observable in both graft groups, which indicated that a subpopulation of recruited, captured, or infiltrated Sca-1$^+$ SPCs had differentiated into α-SMA$^+$ SMCs and had contributed to smooth muscle regeneration. Fewer α-SMA$^+$ Sca-1$^+$ cells were detectable in the PCL group at 2- and 4- weeks post-implantation, yet the ratio of α-SMA$^+$ Sca-1$^+$ cells/Sca-1$^+$ SPCs was similar between the two groups (Fig. 6G). These data further indicated that anti-Sca-1 Ab presentation by grafts increased the presence of Sca-1$^+$ SPCs, and that these cells actively contributed to the accelerated vascular smooth muscle regeneration regardless of graft modification.

3.8. Anti-Sca-1 antibody-functionalized vascular grafts demonstrate an increased presence of M2 macrophages

Macrophages play a critical role in vascular regeneration, stimulating local cells and progenitor cells to recruit and participate in vascular remodelling. Macrophages can be divided into two phenotypes: M1 activated macrophages classically display proinflammatory activity; in contrast, M2 activated macrophages possess the ability to facilitate tissue repair and regeneration [49]. Historically, vascular grafts were designed to promote tissue regeneration and decrease the inflammatory response. The total number of graft-infiltrated macrophages was assessed by anti-CD68 immunofluorescence staining (Fig. 7A). Quantitatively, macrophage-mediated inflammation showed no significant difference in the PCL and PCL-Sca-1 Ab groups, and did not change between 2- and 4- weeks post-implantation (Fig. 7B). These data indicated that modification with anti-Sca-1 antibodies did not aggravate macrophage infiltration compared to unmodified grafts. Furthermore, graft-infiltrated M1 and M2 macrophages were stained using anti-iNOS and anti-CD206 primary antibodies, respectively (Fig. 7C and E). The results showed that the M1 macrophage numbers in PCL-Sca-1 Ab groups were lower than PCL group (Fig. 7D) and more M2 macrophages had infiltrated into the grafts of the PCL-Sca-1 Ab group (Fig. 7F) at 2- and 4- weeks post-implantation, which indicated that surface modification on PCL grafts had an overall beneficial effect on M2 macrophage polarization/infiltration contributing to vascular regeneration.

3.9. Sca-1$^+$ SPCs involved in vascular regeneration are recruited from resident tissues and bone marrow

A bone marrow transplantation (BMT) model was used to address the origin and differentiation of the recipient Sca-1$^+$ SPCs after the implantation of a cell-free vascular graft. Chimeric mice were generated, in which bone marrow cells from GFP transgenic mice were transferred to irradiated *Sca1 2A-CreER; Rosa-RFP* lineage tracing mice (BMT$^{GFP\rightarrow Sca1\ 2A}$) (Fig. 8A). The chimeric mice were then pulsed with tamoxifen and subjected to carotid artery replacement using decellularized allografts due to optimal handing for transplantation (Fig. 8B) or sacrificed for reconstitution analyses. Successful reconstitution of bone marrow in BMT$^{GFP\rightarrow Sca1\ 2A}$ chimeric mice was confirmed by the detection of GFP $^+$ cells in bone marrow by flow cytometry, 6 weeks after bone marrow transplantation (Fig. S11).

The patency of the implanted vascular grafts was examined by Doppler ultrasound at 4 weeks post-implantation (Fig. 8C). Graft explants were first observed by stereoscopic microscopy, which showed that the implanted grafts were patent without thrombosis (Fig. 8D). Furthermore, brightfield and fluorescent images showed that the grafts exhibited both RFP and GFP, which was indicative of the presence of resident SPCs and bone marrow-derived Cells. The data suggested that both types of Sca-1$^+$ cells had migrated into the graft wall and participated in the process of vascular regeneration (Fig. 8E).

Cellularization and tissue regeneration were demonstrated by H&E staining (Fig. 8F). Immunofluorescence staining for Sca-1 (Fig. 8G) indicated the robustness of Sca-1$^+$ SPC numbers that had infiltrated into the grafts (Fig. 8H). The percentage of Sca-1$^+$ SPCs among all cells was 37.39 ± 5.70%, indicating the extensive contribution of Sca-1$^+$ SPCs to graft repopulation and regeneration after implantation.

To further explore the relative contribution of differentially sourced Sca-1$^+$ SPCs to vascular regeneration, co-immunofluorescence staining for Sca-1/GFP or Sca-1/RFP was used to investigate whether Sca-1$^+$ SPCs originated from bone marrow or resident tissues. The results showed fewer Sca-1$^+$ GFP$^+$ cells and more Sca-1$^+$ RFP$^+$ cells repopulated the graft walls (Fig. 8I). Quantitatively, the resident tissue-derived Sca-1$^+$ RFP$^+$ SPCs were distributed in both the adventitia and the lumen of the graft, and the percentage of these cells among all Sca-1$^+$ cells was 74.38 ± 5.60%. The bone marrow-derived Sca-1$^+$ GFP$^+$ SPCs were predominantly distributed within the neo-tissue layer on the lumen side of the graft and had participated in the formation of the neo-artery, with few of these cells distributed within the adventitia. Quantitatively, the percentage of bone marrow-derived Sca-1$^+$ GFP$^+$ SPCs among all Sca-1$^+$ SPCs was 23.90 ± 5.82% (Fig. 8J).

To determine whether a distinct population of recruited Sca-1$^+$ SPCs contributed to certain vascular lineages, immunofluorescence staining was performed by using CD31 (green) and Sca-1 (red) antibodies. The results revealed that a subset of CD31$^+$ cells in the endothelial layer and capillaries of the graft wall were colocalized with Sca-1$^+$, indicating that they were derived from Sca-1$^+$ SPCs. Meanwhile, we analysed the distribution of the α-SMA$^+$ Sca-1$^+$ cells in the vascular grafts by immunofluorescence staining with α-SMA (green) and Sca-1 (red) antibodies (Fig. 8K). The results showed that a significant portion of cells expressing Sca-1$^+$ were α-SMA$^+$ cells in the implanted vascular graft, indicating that α-SMA$^+$ Sca-1$^+$ cells were derived from Sca-1$^+$ SPCs. The differentiation ratios of Sca-1$^+$ SPCs towards ECs and SMCs were calculated (Fig. 8L), and the results revealed that Sca-1$^+$ SPCs contribute to the endothelialization and smooth muscle regeneration of vascular grafts.

4. Discussion

Vascular grafts fabricated from synthetic polymers are promising candidates for the development of tissue-engineered vascular grafts.

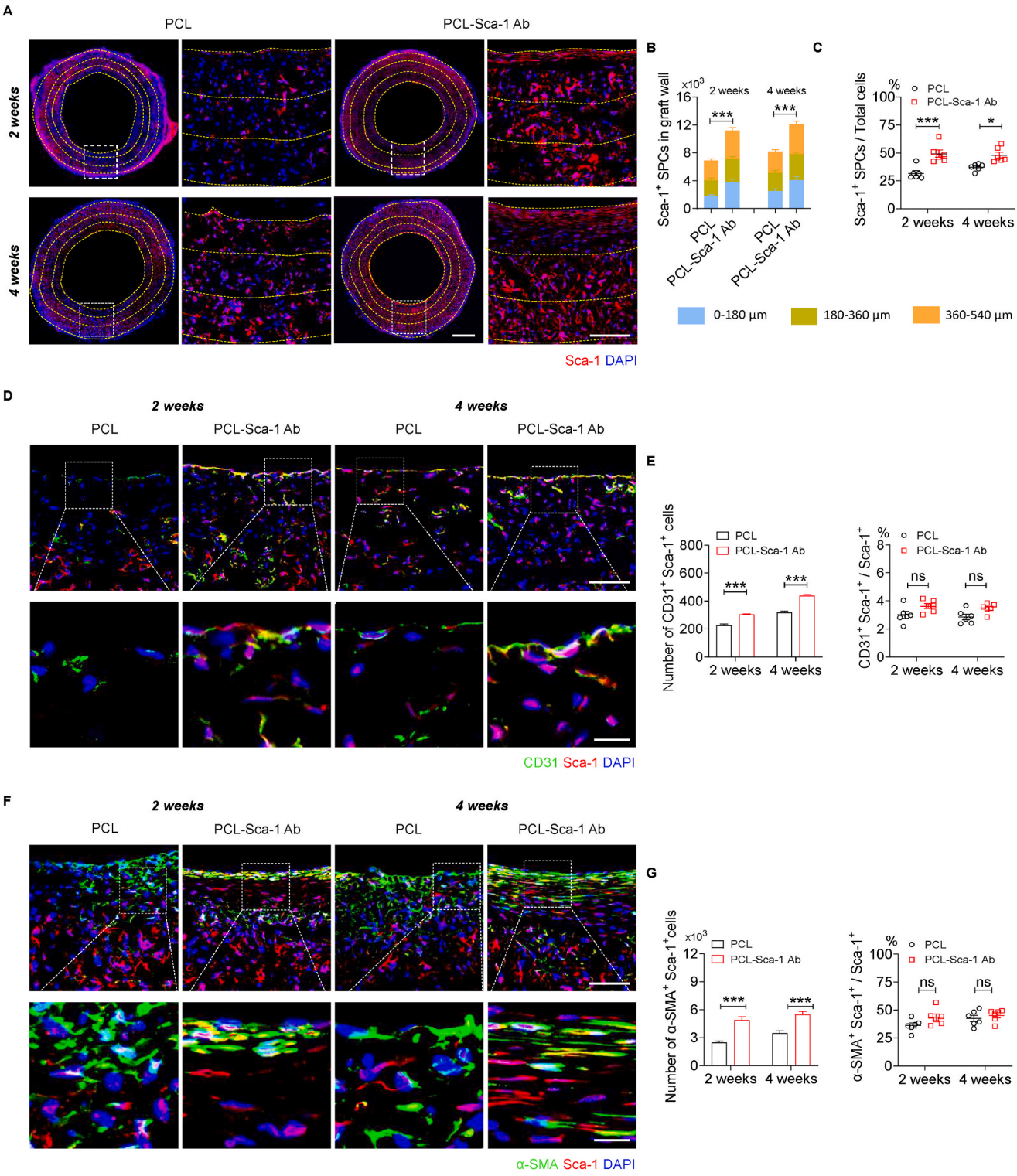

Fig. 6. Anti-Sca-1 antibody modification increases the infiltration of Sca-1$^+$ SPCs and enhances endothelialization and smooth muscle regeneration. (A) The distribution of Sca-1$^+$ SPCs in the vascular graft wall at 2- and 4- weeks post-implantation was shown by immunofluorescence staining with Sca-1 antibody. Nuclei were stained with DAPI. Yellow dashed lines indicate the areas at 0–180 μm, 180–360 μm and 360–540 μm graft depths from the graft lumen. Scale bars, 500 μm or 100 μm (magnified images). (B) The number of Sca-1$^+$ SPCs within the vascular graft wall at 0–180 μm, 180–360 μm and 360–540 μm depths from the luminal surface was calculated based on Sca-1 immunofluorescence staining, as well as (C) the ratio of Sca-1$^+$ SPCs to total cells. Data were expressed as mean ± s.e.m. for each group: $^*p < 0.05$, $^{***}p < 0.001$. (D) Co-immunofluorescence staining of Sca-1 and CD31 in the vascular graft wall at 2- and 4- weeks post-implantation. Scale bars, 100 μm or 20 μm (magnified images). (E) Quantification of the number of Sca-1$^+$ CD31$^+$ cells and the ratio of CD31$^+$ cells in Sca-1$^+$ SPCs in the vascular grafts. Data were expressed as mean ± s.e.m. for each group: $^{***}p < 0.001$. (F) Co-immunofluorescence staining of Sca-1 and α-SMA in the vascular graft wall at 2- and 4- weeks post-implantation. Scale bars, 100 μm or 20 μm (magnified images). (G) Quantification of the number of Sca-1+ α-SMA + cells and the ratio of α-SMA$^+$ cells in Sca-1$^+$ SPCs in the vascular grafts. Data were expressed as mean ± s.e.m. for each group: $^{***}p < 0.001$. Images and data are representative of n = 6 independent experiments. (For interpretation of the references to colour in this figure legend, the reader is referred to the Web version of this article.)

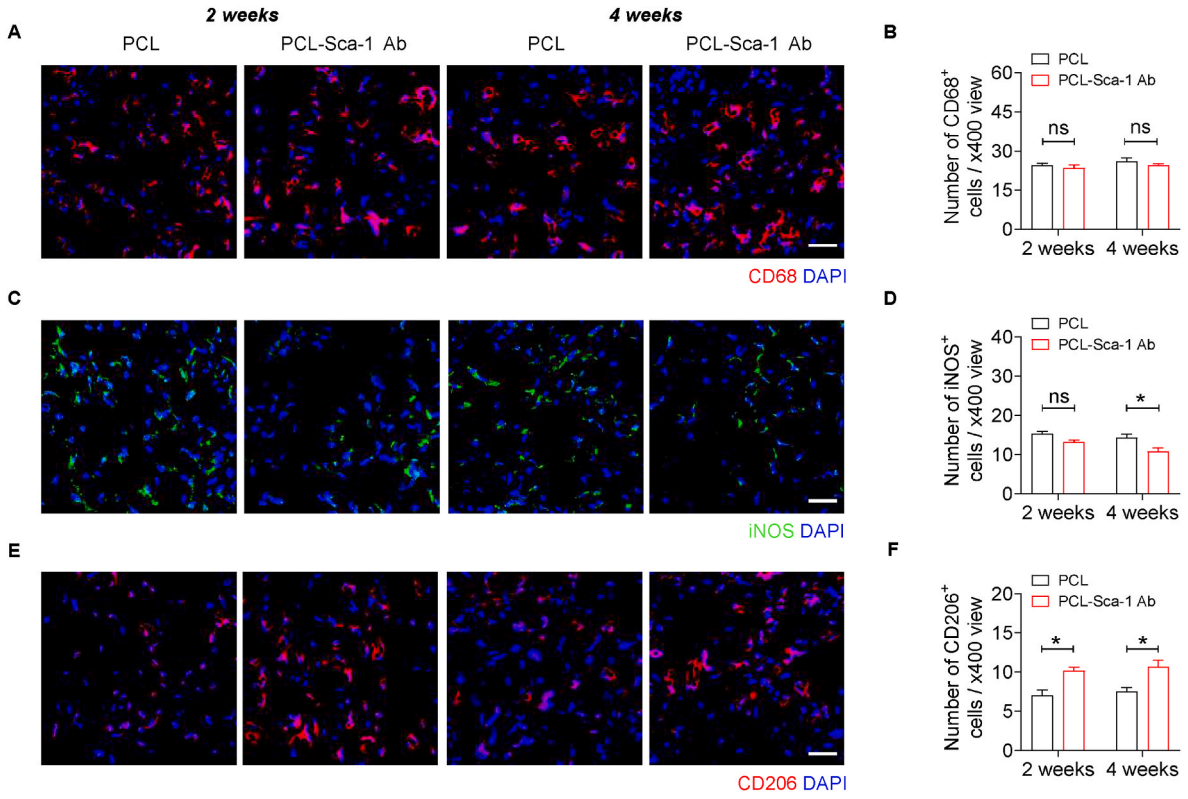

Fig. 7. Anti-Sca-1 antibody-functionalized vascular grafts demonstrate an increased presence of M2 macrophages. (A, C and E) Representative immunofluorescence images of cross-sections of implanted grafts with anti-CD68, anti-iNOS and anti-CD206 antibodies at 2- and 4-weeks post-implantation. Scale bar, 50 μm. (B, D and F) Quantitative analyses of the number of $CD68^+$, $iNOS^+$ and $CD206^+$ cells per view. Data were expressed as mean ± s.e.m. for each group: $^*p < 0.05$. Images and data are representative of n = 6 independent experiments.

However, there remains limited data on the translational implementation of small-diameter vascular grafts in clinical trials due to the bioinert characteristics and pre-clinical complications observed with synthetic polymer vascular grafts [50]. Synthetic polymers lack the biological activity necessary to induce timely tissue regeneration, which may trigger a cascade of pathogenic cellular and molecular events, including prolonged inflammation, thrombogenic reactions, smooth muscle cell hyperproliferation and activation, and poor re-endothelialization. Thus, the resulting intimal hyperplasia, restenosis and thrombosis ultimately result in synthetic polymer vascular graft implant failure. Hence, there has been increasing attention given to the development of approaches to improve the translational performance of small-diameter vascular grafts, including polymer surface modification [51–54], polymer blending [55], or functionalization to convey the controlled release of effector molecules (e.g., nitric oxide) [17,56,57] and therapeutics [58,59]. In this study, we performed a new type of bioactive modification of PCL vascular grafts to modulate *in situ* progenitor cell responses conducive to vascular regeneration.

Research into the reendothelialization of vascular grafts with autologous endothelial cells prior to implantation continues to be a developing approach. However, the associated procedures are extremely time-, labour- and cost-intensive. Whilst promising results have been obtained, their proven success in clinical cases is limited. Modification of scaffold materials with antibodies aims to increase the recruitment and capture of cells for scaffold seeding *in situ*. Capture of cells using anti-CD34 antibodies was previously demonstrated to enhance reendothelialization *in vivo* but also promoted intimal hyperplasia [60]. This outcome may have been related to the antibody competitively binding CD34, a known ligand for selectins and mediating cell tethering and cell-cell interactions [61]. It has previously been established that both local resident and circulating stem/progenitor cells contribute to vascular remodelling following vascular injury [31,62–64]. Vascular SPCs are mostly quiescent in their niches but can be activated in response to injury and participate in endothelial repair and smooth muscle cell accumulation to form neointima [65]. In the adventitia, abundant SPCs expressing $Sca\text{-}1^+$ have been identified; they can migrate towards implanted grafts, where they further differentiate into either ECs or SMCs depending on the specific microenvironment or stimuli [13,29,41]. Therefore, in the present study, we developed an electrospun vascular graft immobilized anti-Sca-1 antibody surface modification. The anti-Sca-1 antibody-functionalized grafts enhanced the recruitment, capture and retainment of $Sca\text{-}1^+$ SPCs *in vitro,* and their feasibility as vascular grafts *in vivo* was demonstrated in rat abdominal aorta replacement models. Anti-Sca-1 antibody-functionalized vascular grafts demonstrated enhanced vascular tissue regeneration compared to the control grafts, including rapid endothelialization and timely regeneration of robust and organized smooth muscle layers.

Anti-Sca-1 antibody-functionalized vascular grafts exhibited the highest attachment number of $Sca\text{-}1^+$ SPCs among the four types of mats assessed. We observed that PCL-Biotin and PCL-Biotin-Avidin mats tended to increase the number of adhered $Sca\text{-}1^+$ SPCs. This phenomenon could be attributed to the improved hydrophilicity of the surface of the PCL mats after biotin/avidin modifications. Increased hydrophilicity of material surfaces has been shown to be favourable to the adhesion, proliferation, and migration of cells [66]. Even so, we showed that the number of adhered $Sca\text{-}1^+$ SPCs was not significantly different compared to blank PCL mats, which further justified the additional requirement of an active capture mechanism. Our data suggested that the increased attachment of $Sca\text{-}1^+$ SPCs was due to the specific modification of PCL to display anti-Sca-1 antibodies. Indeed, our dynamic culture system further verified the benefits of anti-Sca-1 antibody presentation on the lumen of the electrospun graft scaffolds. Interestingly, cell retainment under flow showed that $Sca\text{-}1^+$ SPCs were stably adhered to the lumen surface of PCL-Sca-1 Ab grafts and remained adherent

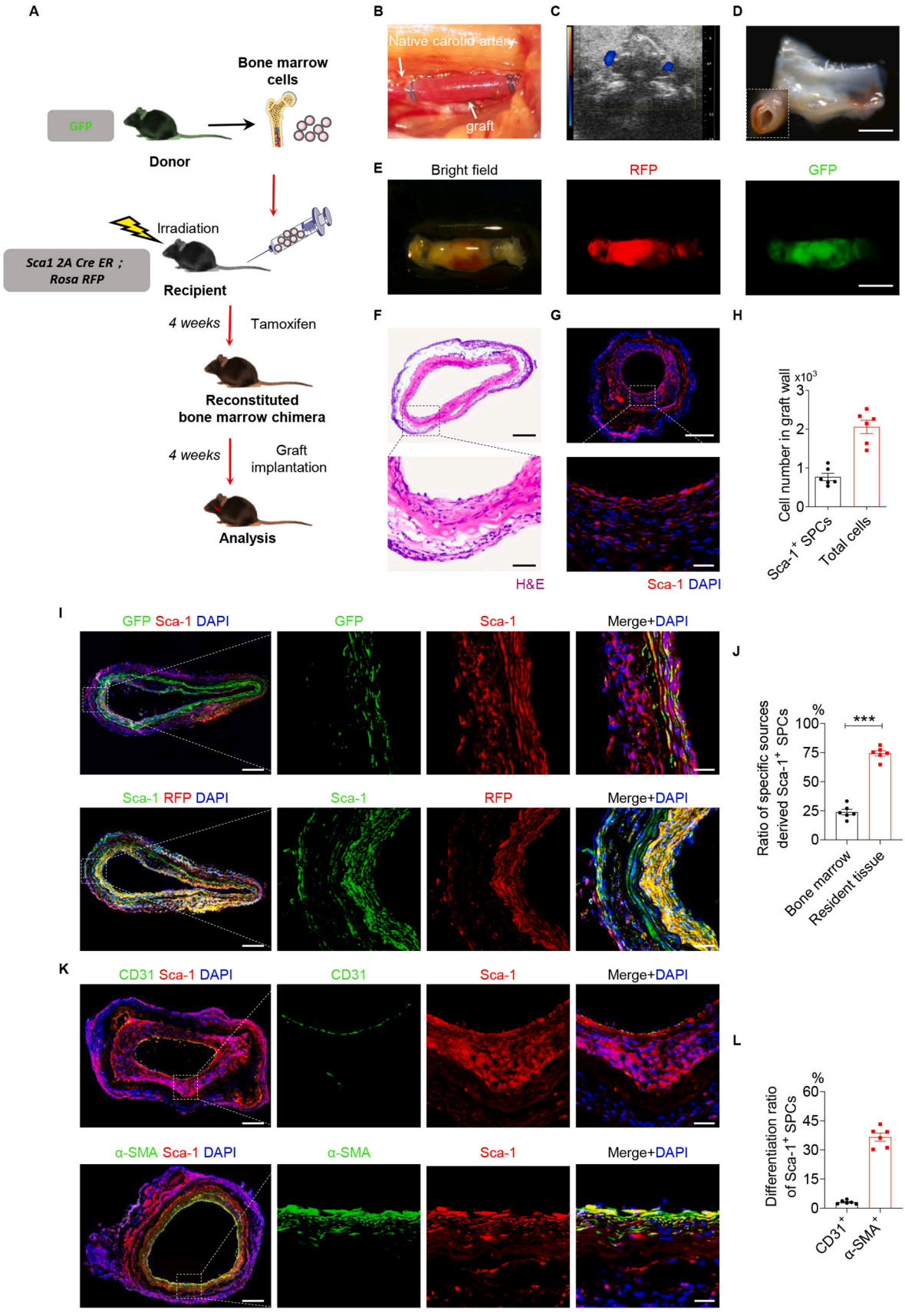

(caption on next page)

Fig. 8. Sca-1$^+$ SPCs contribute to the endothelialization and smooth muscle regeneration of vascular grafts in a bone marrow transplantation (BMT) mouse model. (A) Schematic illustration showing that a BMT model was constructed by transplanting GFP$^+$ bone marrow cells into Sca1 2A CreER; Rosa-RFP lineage tracing mouse. (B) Representative stereoscopic image of vascular graft after implantation. (C) Representative Doppler ultrasound image of the implanted graft. (D) The luminal surface of the explanted graft was observed by stereomicroscopy. Scale bar, 1 mm. (E) Bright-field and fluorescence images of vascular grafts after explantation. Scale bar, 2 mm. H&E (F) and immunofluorescence (G) staining of Sca-1 in vascular grafts at 4 weeks post-implantation in the BMT mice. Scale bars, 500 μm or 50 μm (magnified images). (H) Quantitative analyses of the Sca-1$^+$ SPCs and total cell number in the graft wall. Data were expressed as mean ± s.e.m. for each group. (I) Co-immunofluorescence staining of GFP/Sca-1 and RFP/Sca-1 in vascular grafts at 4 weeks post-implantation. Scale bars, 200 μm or 50 μm (magnified images). (J) Quantitative analysis of the ratio of Sca-1$^+$ SPCs derived from specific sources in total Sca-1$^+$ SPCs. Data were expressed as mean ± s.e.m. for each group: ***$p <$ 0.001. (K) Co-immunofluorescence staining of Sca-1/CD31 and Sca-1/α-SMA in vascular grafts at 4 weeks post-implantation. Scale bars, 200 μm or 50 μm (magnified images). (L) Quantification of the ratio of CD31$^+$ cells in Sca-1$^+$ SPCs, and the ratio of α-SMA$^+$ cells in Sca-1$^+$ SPCs in the vascular graft. Data were expressed as mean ± s.e.m. for each group. Images and data are representative of n = 6 independent experiments.

under constant exposure to shear stress over 6 h. Coupled with the demonstrated support for seeded cell growth, our grafts may also hold promise if pre-seeded with Sca-1$^+$ SPCs prior to implantation, an avenue that informs our future research direction.

Previous studies showed that Sca-1$^+$ SPCs harbored the potential for reparative and regenerative processes by differentiating into ECs or SMCs to participate in endothelial/smooth muscle layer regeneration [67] and promote atherosclerotic plaque stability [12]. Our results also revealed that Sca-1$^+$ SPCs had differentiated into ECs or SMCs during the regeneration process *in vivo*. In the present study, CD31$^+$ Sca-1$^+$ double immunofluorescence indicated cells positive for both markers, indicative of SPC-derived ECs. Zeng et al. demonstrated that stem cells differentiated into ECs under the effect of shear stress stimuli [68]. Hence, given that the endothelialization process was markedly enhanced in the PCL-Sca-1 Ab groups compared to the PCL groups, we inferred that anti-Sca-1 antibody-functionalized vascular graft recruitment and capture of Sca-1$^+$ SPCs enriched a subset of Sca-1$^+$ SPCs to differentiate into ECs, potentially under the shear stress stimuli from blood flow.

Timely acquisition of a contractile SMC layer helps to maintain the vessel tone necessary for the long-term function and patency of implanted grafts [69]. Zhou et al. provided considerable evidence that a Sca-1$^+$ SPC population contributed to approximately 40% of the SMCs in some regions of the vessel wall, further delineating the critical roles of SPC subsets in vessel repair and functional recovery after injury [31].

Our own data revealed that anti-Sca-1 antibody-functionalized vascular grafts markedly increased the thickness of organized SMC layers that were positive for the marker of contractile SMCs (SM-MHC) at 4 weeks post-implantation. Our study suggested that a significant proportion of the captured Sca-1$^+$ SPCs attached and contributed to the regenerated ECM-abundant SMC layer, as evidenced by α-SMA$^+$ Sca-1$^+$ cells. However, we also observed α-SMA$^+$ Sca-1$^+$ cells distal to the luminal side of the neo-tissue and proximal to the graft wall, which we speculate to be suggestive of Sca-1$^+$ SPC recruitment from resident tissues and contribution to the SMC layer. This may recapitulate the adventitia-resident Sca-1$^+$ SPC directional migration toward the neointima that was previously observed in vein graft studies [70].

In light of our data indicating an abundant Sca-1$^+$ SPC response in the repopulation and regeneration of implanted vascular grafts in rat abdominal aorta replacement models, we then sought to determine the source of these Sca-1$^+$ SPCs. For this purpose, we used a bone marrow transplantation mouse carotid artery replacement model, and further explored the source and vascular lineage fate of Sca-1$^+$ SPCs resident to the resident tissues or recruited from the bone marrow. The transgenic and irradiated mouse models demonstrated the participation of Sca-1$^+$ SPCs resident to the surrounding tissues (RFP$^+$) and a population of Sca-1$^+$ SPCs recruited from the bone marrow (GFP$^+$ cells from donor mice). Consistent with the above views, the regeneration mechanisms and localization of Sca-1$^+$ SPCs observed in our PCL-Sca-1 Ab grafts in rat models reflected that the recruitment of Sca-1$^+$ SPCs from both resident tissues and bone marrow contributed to enhanced vascular regeneration.

Electrospun PCL vascular grafts are promising contenders for realizing off-the-shelf and readily available artificial blood vessels that provide appropriate mechanical properties and maintenance of patency. Besides, material degradation has been accepted a key factor affecting the regeneration and long term performance of cell-free vascular grafts [71]. Electrospun PCL vascular grafts have been reported to exhibit notable degradation, including fiber fragmentation and reduction of molecular weight, after 18 months in a rat abdominal aorta replacement model [72]. Furthermore, the balance between material degradation, maintained mechanical support, and tissue regeneration effect remains a significant challenge in achieving long-term vascular graft performance.

5. Conclusion

Here, we successfully designed and fabricated PCL vascular grafts modified with biotin/avidin-conjugated anti-Sca-1 antibodies. Anti-Sca-1 antibody-functionalized vascular grafts specifically promoted the attachment and retention of Sca-1$^+$ SPCs under static and dynamic flow culture conditions *in vitro*. The performance of our grafts was assessed in rat abdominal aorta replacement models, which demonstrated that anti-Sca-1 antibody-functionalized vascular grafts elicited a rapid process of reendothelialization and smooth muscle layer regeneration through the active recruitment and capture of Sca-1$^+$ SPCs from resident tissues and circulation. The abundance of recruited/captured SPCs contributed EC and SMC lineages and enhanced the formation of neo-tissue that closely resembled native arterial tissue. The regeneration mechanism of Sca-1$^+$ SPCs was further investigated by using a bone marrow transplantation carotid artery replacement mouse model. The data suggested that Sca-1$^+$ SPCs originating from resident tissues and bone marrow infiltrated into vascular grafts and contributed to rapid vascular regeneration by differentiating into vascular cell lineages and contributing to vascular layer regeneration. In summary, our PCL-Sca-1 Ab grafts offer a novel approach to functionalization of polymer vascular grafts and serve as promising candidates for pro-regenerative small-diameter vascular graft implants.

CRediT authorship contribution statement

He Wang: Investigation, Methodology, Formal analysis, Data curation, Writing – original draft. **Mengmeng Xing:** Investigation, Formal analysis, Data curation. **Weiliang Deng:** Investigation. **Meng Qian:** Investigation. **Fei Wang:** Investigation, Methodology. **Kai Wang:** Methodology. **Adam C. Midgley:** Writing – review & editing. **Qiang Zhao:** Conceptualization, Writing – review & editing, Supervision, Funding acquisition.

Declaration of competing interest

The authors declare no conflict of interest.

Acknowledgements

This study was supported by grants from the National Natural Science Foundation of China (Nos. 81925021, 82050410449, 81921004 and 81871500) and Science & Technology Project of Tianjin of China (No. 18JCJQJC46900).

Appendix A. Supplementary data

Supplementary data to this article can be found online at https://doi.org/10.1016/j.bioactmat.2022.03.007.

References

[1] M. Arsalan, M.J. Mack, Coronary artery bypass grafting is currently underutilized, Circulation 133 (10) (2016) 1036–1045, https://doi.org/10.1161/Circulationaha.115.018032.

[2] R.Y. Kannan, et al., Current status of prosthetic bypass grafts: a review, J. Biomed. Mater. Res. B 74b (1) (2005) 570–581, https://doi.org/10.1002/jbm.b.30247.

[3] S.L. Dahl, et al., Readily available tissue-engineered vascular grafts, Sci. Transl. Med. 3 (68) (2011) 68ra9, https://doi.org/10.1126/scitranslmed.3001426.

[4] R.C. Goncalves, et al., Strategies for re-vascularization and promotion of angiogenesis in trauma and disease, Biomaterials 269 (2021) 120628, https://doi.org/10.1016/j.biomaterials.2020.120628.

[5] R.D. Kirkton, et al., Bioengineered human acellular vessels recellularize and evolve into living blood vessels after human implantation, Sci. Transl. Med. 11 (485) (2019), https://doi.org/10.1126/scitranslmed.aau6934.

[6] D.G. Seifu, et al., Small-diameter vascular tissue engineering, Nat. Rev. Cardiol. 10 (7) (2013) 410–421, https://doi.org/10.1038/nrcardio.2013.77.

[7] T. Sugiura, et al., Fast-degrading bioresorbable arterial vascular graft with high cellular infiltration inhibits calcification of the graft, J. Vasc. Surg. 66 (1) (2017) 243–250, https://doi.org/10.1016/j.jvs.2016.05.096.

[8] S. Enomoto, et al., Long-term patency of small-diameter vascular graft made from fibroin, a silk-based biodegradable material, J. Vasc. Surg. 51 (1) (2010) 155–164, https://doi.org/10.1016/j.jvs.2009.09.005.

[9] S. Lu, et al., Synthetic ePTFE grafts coated with an anti-CD133 antibody-functionalized heparin/collagen multilayer with rapid in vivo endothelialization properties, Acs Appl. Mater. Inter. 5 (15) (2013) 7360–7369, https://doi.org/10.1021/am401706w.

[10] M. Wen, et al., Local delivery of dual microRNAs in trilayered electrospun grafts for vascular regeneration, Acs Appl. Mater. Inter. 12 (6) (2020) 6863–6875, https://doi.org/10.1021/acsami.9b19452.

[11] N. Hibino, et al., Tissue-engineered vascular grafts form neovessels that arise from regeneration of the adjacent blood vessel, Faseb. J. 25 (8) (2011) 2731–2739, https://doi.org/10.1096/fj.11-182246.

[12] E. Karamariti, et al., DKK3 (dickkopf 3) alters atherosclerotic plaque phenotype involving vascular progenitor and fibroblast differentiation into smooth muscle cells, Arterioscl. Throm. Vas. 38 (2) (2018) 425–437, https://doi.org/10.1161/Atvbaha.117.310079.

[13] Y. Pan, et al., Histone deacetylase 7-derived peptides play a vital role in vascular repair and regeneration, Adv. Sci. 5 (8) (2018) 1800006, https://doi.org/10.1002/advs.201800006.

[14] Z. Wang, et al., The effect of thick fibers and large pores of electrospun poly (epsilon-caprolactone) vascular grafts on macrophage polarization and arterial regeneration, Biomaterials 35 (22) (2014) 5700–5710, https://doi.org/10.1016/j.biomaterials.2014.03.078.

[15] Q. Yang, et al., A novel biodegradable external stent regulates vein graft remodeling via the Hippo-YAP and mTOR signaling pathways, Biomaterials 258 (2020) 120254, https://doi.org/10.1016/j.biomaterials.2020.120254.

[16] W. Gong, et al., Hybrid small-diameter vascular grafts: anti-expansion effect of electrospun poly epsilon-caprolactone on heparin-coated decellularized matrices, Biomaterials 76 (2016) 359–370, https://doi.org/10.1016/j.biomaterials.2015.10.066.

[17] Z. Wang, et al., Enzyme-functionalized vascular grafts catalyze in-situ release of nitric oxide from exogenous NO prodrug, J. Contr. Release 210 (2015) 179–188, https://doi.org/10.1016/j.jconrel.2015.05.283.

[18] Q. Zhao, et al., Polysaccharide-based biomaterials with on-demand nitric oxide releasing property regulated by enzyme catalysis, Biomaterials 34 (33) (2013) 8450–8458, https://doi.org/10.1016/j.biomaterials.2013.07.045.

[19] K. Wang, et al., Enhanced vascularization in hybrid PCL/gelatin fibrous scaffolds with sustained release of VEGF, BioMed Res. Int. 2015 (2015) 865076, https://doi.org/10.1155/2015/865076.

[20] X. Chen, et al., Electrospun poly(L-lactic acid-co-varepsilon-caprolactone) fibers loaded with heparin and vascular endothelial growth factor to improve blood compatibility and endothelial progenitor cell proliferation, Colloids Surf. B Biointerfaces 128 (2015) 106–114, https://doi.org/10.1016/j.colsurfb.2015.02.023.

[21] M.T. Conconi, et al., Effects on in vitro and in vivo angiogenesis induced by small peptides carrying adhesion sequences, J. Pept. Sci. 16 (7) (2010) 349–357, https://doi.org/10.1002/psc.1251.

[22] M. Avci-Adali, et al., New strategies for in vivo tissue engineering by mimicry of homing factors for self-endothelialisation of blood contacting materials, Biomaterials 29 (29) (2008) 3936–3945, https://doi.org/10.1016/j.biomaterials.2008.07.002.

[23] Z. Li, et al., Pretargeting and bioorthogonal click chemistry-mediated endogenous stem cell homing for heart repair, ACS Nano 12 (12) (2018) 12193–12200, https://doi.org/10.1021/acsnano.8b05892.

[24] Y. Duan, et al., Co-immobilization of CD133 antibodies, vascular endothelial growth factors, and REDV peptide promotes capture, proliferation, and differentiation of endothelial progenitor cells, Acta Biomater. 96 (2019) 137–148, https://doi.org/10.1016/j.actbio.2019.07.004.

[25] T. Shirota, et al., Fabrication of endothelial progenitor cell (EPC)-seeded intravascular stent devices and in vitro endothelialization on hybrid vascular tissue, Biomaterials 24 (13) (2003) 2295–2302, https://doi.org/10.1016/s0142-9612(03)00042-5.

[26] Q. Xu, et al., Circulating progenitor cells regenerate endothelium of vein graft atherosclerosis, which is diminished in ApoE-deficient mice, Circ. Res. 93 (8) (2003) E76–E86, https://doi.org/10.1161/01.Res.0000097864.24725.60.

[27] A. Briasoulis, et al., The role of endothelial progenitor cells in vascular repair after arterial injury and atherosclerotic plaque development, Cardiovasc. Ther. 29 (2) (2011) 125–139, https://doi.org/10.1111/j.1755-5922.2009.00131.x.

[28] M. Sata, et al., Hematopoietic stem cells differentiate into vascular cells that participate in the pathogenesis of atherosclerosis, Nat. Med. 8 (4) (2002) 403–409, https://doi.org/10.1038/nm0402-403.

[29] Y. Hu, et al., Abundant progenitor cells in the adventitia contribute to atherosclerosis of vein grafts in ApoE-deficient mice, J. Clin. Invest. 113 (9) (2004) 1258–1265, https://doi.org/10.1172/JCI19628.

[30] I. Kokkinopoulos, et al., Adventitial SCA-1(+) progenitor cell gene sequencing reveals the mechanisms of cell migration in response to hyperlipidemia, Stem Cell Rep. 9 (2) (2017) 681–696, https://doi.org/10.1016/j.stemcr.2017.06.011.

[31] J. Tang, et al., Arterial sca1(+) vascular stem cells generate de novo smooth muscle for artery repair and regeneration, Cell Stem Cell 26 (1) (2020) 81–96, https://doi.org/10.1016/j.stem.2019.11.010, e4.

[32] M.M. Wong, et al., Sirolimus stimulates vascular stem/progenitor cell migration and differentiation into smooth muscle cells via epidermal growth factor receptor/extracellular signal-regulated kinase/beta-catenin signaling pathway, Arterioscl. Throm. Vas. 33 (10) (2013) 2397–2406, https://doi.org/10.1161/Atvbaha.113.301595.

[33] P. Campagnolo, et al., c-Kit+ progenitors generate vascular cells for tissue-engineered grafts through modulation of the Wnt/Klf4 pathway, Biomaterials 60 (2015) 53–61, https://doi.org/10.1016/j.biomaterials.2015.04.055.

[34] B.D. Markway, et al., Capture of flowing endothelial cells using surface-immobilized anti-kinase insert domain receptor antibody, Tissue Eng. C Methods 14 (2) (2008) 97–105, https://doi.org/10.1089/ten.tec.2007.0300.

[35] J. Zhang, et al., ECM-mimetic heparin glycosamioglycan-functionalized surface favors constructing functional vascular smooth muscle tissue in vitro, Colloids Surf. B Biointerfaces 146 (2016) 280–288, https://doi.org/10.1016/j.colsurfb.2016.06.023.

[36] Q. Ji, et al., Dual functionalization of poly(epsilon-caprolactone) film surface through supramolecular assembly with the aim of promoting in situ endothelial progenitor cell attachment on vascular grafts, Biomacromolecules 14 (11) (2013) 4099–4107, https://doi.org/10.1021/bm401239a.

[37] DI Deo, et al., Biofunctionalization of PEGylated microcapsules for exclusive binding to protein substrates, Biomacromolecules 15 (7) (2014) 2555–2562, https://doi.org/10.1021/bm500412d.

[38] T. Kamperman, et al., Spatiotemporal material functionalization via competitive supramolecular complexation of avidin and biotin analogs, Nat. Commun. 10 (1) (2019) 4347, https://doi.org/10.1038/s41467-019-12390-4.

[39] J.D. Clapper, et al., Biotinylated biodegradable nanotemplated hydrogel networks for cell interactive applications, Biomacromolecules 9 (4) (2008) 1188–1194, https://doi.org/10.1021/bm701176j.

[40] R. Murthy, C.E. Shell, Grunlan MA, The influence of poly(ethylene oxide) grafting via siloxane tethers on protein adsorption, Biomaterials 30 (13) (2009) 2433–2439, https://doi.org/10.1016/j.biomaterials.2009.01.051.

[41] S Issa Bhaloo, et al., Binding of dickkopf-3 to CXCR7 enhances vascular progenitor cell migration and degradable graft regeneration, Circ. Res. 123 (4) (2018) 451–466, https://doi.org/10.1161/CIRCRESAHA.118.312945.

[42] K. Qin, et al., Hyaluronan promotes the regeneration of vascular smooth muscle with potent contractile function in rapidly biodegradable vascular grafts, Biomaterials 257 (2020) 120226, https://doi.org/10.1016/j.biomaterials.2020.120226.

[43] A. Lancuski, S. Fort, F. Bossard, Electrospun azido-PCL nanofibers for enhanced surface functionalization by click chemistry, Acs Appl. Mater. Inter 4 (12) (2012) 6499–6504, https://doi.org/10.1021/am301458y.

[44] A. Lancuski, F. Bossard, S. Fort, Carbohydrate-decorated PCL fibers for specific protein adhesion, Biomacromolecules 14 (6) (2013) 1877–1884, https://doi.org/10.1021/bm400263d.

[45] N.L. Heureux, et al., Human tissue-engineered blood vessels for adult arterial revascularization, Nat. Med. 12 (3) (2006) 361–365, https://doi.org/10.1038/nm1364.

[46] F. Chen, C.N. Lee, S.H. Teoh, Nanofibrous modification on ultra-thin poly(epsilon-caprolactone) membrane via electrospinning, Mat. Sci. Eng. C-Bio S 27 (2) (2007) 325–332, https://doi.org/10.1016/j.msec.2006.05.004.

[47] A.C. Strang, et al., Superior in vivo compatibility of hydrophilic polymer coated prosthetic vascular grafts, J. Vasc. Access 15 (2) (2014) 95–101, https://doi.org/10.5301/jva.5000166.

[48] M. Weber, et al., Blood-contacting biomaterials: in vitro evaluation of the hemocompatibility, Front. Bioeng. Biotechnol. 6 (2018) 99, https://doi.org/10.3389/fbioe.2018.00099.

[49] B.N. Brown, et al., Macrophage phenotype and remodeling outcomes in response to biologic scaffolds with and without a cellular component, Biomaterials 30 (8) (2009) 1482–1491, https://doi.org/10.1016/j.biomaterials.2008.11.040.

[50] Juncos LI, S. Textor, Current approaches to atherosclerotic obstructive renal artery stenosis, Ther. Adv. Cardiovasc. Dis. 9 (4) (2015) 153–157, https://doi.org/10.1177/1753944715579143.

[51] Q. Lin, et al., In situ endothelialization of intravascular stents coated with an anti-CD34 antibody functionalized heparin-collagen multilayer, Biomaterials 31 (14) (2010) 4017–4025, https://doi.org/10.1016/j.biomaterials.2010.01.092.
[52] P.H. Blit, et al., Platelet inhibition and endothelial cell adhesion on elastin-like polypeptide surface modified materials, Biomaterials 32 (25) (2011) 5790–5800, https://doi.org/10.1016/j.biomaterials.2011.04.067.
[53] W. Wu, R.A. Allen, Y. Wang, Fast-degrading elastomer enables rapid remodeling of a cell-free synthetic graft into a neoartery, Nat. Med. 18 (7) (2012) 1148–1153, https://doi.org/10.1038/nm.2821.
[54] Y. Yang, et al., Hybrid electrospun rapamycin-loaded small-diameter decellularized vascular grafts effectively inhibit intimal hyperplasia, Acta Biomater. 97 (2019) 321–332, https://doi.org/10.1016/j.actbio.2019.06.037.
[55] Y. Hong, et al., A small diameter, fibrous vascular conduit generated from a poly (ester urethane)urea and phospholipid polymer blend, Biomaterials 30 (13) (2009) 2457–2467, https://doi.org/10.1016/j.biomaterials.2009.01.013.
[56] H. Jun, L. Taite, J. West, Nitric oxide-producing polyurethanes, Biomacromolecules 6 (2) (2005) 838–844, https://doi.org/10.1021/bm049419y.
[57] L.J. Taite, et al., Nitric oxide-releasing polyurethane-PEG copolymer containing the YIGSR peptide promotes endothelialization with decreased platelet adhesion, J. Biomed. Mater. Res. B 84b (1) (2008) 108–116, https://doi.org/10.1002/jbm.b.30850.
[58] C. Del Gaudio, et al., Aspirin-loaded electrospun poly(epsilon-caprolactone) tubular scaffolds: potential small-diameter vascular grafts for thrombosis prevention, J. Mater. Sci. Mater. Med. 24 (2) (2013) 523–532, https://doi.org/10.1007/s10856-012-4803-3.
[59] F. Innocente, et al., Paclitaxel-eluting biodegradable synthetic vascular prostheses: a step towards reduction of neointima formation, Circulation 120 (11) (2009) S37–S45, https://doi.org/10.1161/Circulationaha.109.848242.
[60] J.I. Rotmans, et al., In vivo cell seeding with anti-CD34 antibodies successfully accelerates endothelialization but stimulates intimal hyperplasia in porcine arteriovenous expanded polytetrafluoroethylene grafts, Circulation 112 (1) (2005) 12–18, https://doi.org/10.1161/Circulationaha.104.504407.
[61] A.W. Greenberg, W.G. Kerr, D.A. Hammer, Relationship between selectin-mediated rolling of hematopoietic stem and progenitor cells and progression in hematopoietic development, Blood 95 (2) (2000) 478–486, https://doi.org/10.1182/blood.V95.2.478.
[62] A. Le Bras, et al., Adventitial sca1+cells transduced with ETV2 are committed to the endothelial fate and improve vascular remodeling after injury, Arterioscl Throm Vas 38 (1) (2018) 232–244, https://doi.org/10.1161/Atvbaha.117.309853.
[63] Z. Ni, et al., Recipient c-Kit lineage cells repopulate smooth muscle cells of transplant arteriosclerosis in mouse models, Circ. Res. 125 (2) (2019) 223–241, https://doi.org/10.1161/Circresaha.119.314855.
[64] L. Zhang, Q. Xu, Stem/Progenitor cells in vascular regeneration, Arterioscler. Thromb. Vasc. Biol. 34 (6) (2014) 1114–1119, https://doi.org/10.1161/ATVBAHA.114.303809.
[65] L. Zhang, et al., Role of resident stem cells in vessel formation and arteriosclerosis, Circ. Res. 122 (11) (2018) 1608–1624, https://doi.org/10.1161/CIRCRESAHA.118.313058.
[66] X. Ren, et al., Surface modification and endothelialization of biomaterials as potential scaffolds for vascular tissue engineering applications, Chem. Soc. Rev. 44 (15) (2015), https://doi.org/10.1039/c5cs90066b, 5745-5745.
[67] M.M. Wong, et al., Macrophages control vascular stem/progenitor cell plasticity through tumor necrosis factor-alpha-mediated nuclear factor-kappaB activation, Arterioscl. Throm. Vas. 34 (3) (2014) 635–643, https://doi.org/10.1161/Atvbaha.113.302568.
[68] L. Zeng, et al., HDAC3 is crucial in shear- and VEGF-induced stem cell differentiation toward endothelial cells, J. Cell Biol. 174 (7) (2006) 1059–1069, https://doi.org/10.1083/jcb.200605113.
[69] M.B. Chan-Park, et al., Biomimetic control of vascular smooth muscle cell morphology and phenotype for functional tissue-engineered small-diameter blood vessels (vol 88a, pg 1104, 2009), J. Biomed. Mater. Res. 91a (2) (2009) 629–634, https://doi.org/10.1002/jbm.a.32597.
[70] B. Yu, et al., Vascular stem/progenitor cell migration induced by smooth muscle cell-derived chemokine (c-c Motif) ligand 2 and chemokine (c-x-c motif) ligand 1 contributes to neointima formation, Stem Cell. 34 (9) (2016) 2368–2380, https://doi.org/10.1002/stem.2410.
[71] Y. Wei, et al., Tissue-engineered vascular grafts and regeneration mechanisms, J. Mol. Cell. Cardiol. 165 (2021) 40–53, https://doi.org/10.1016/j.yjmcc.2021.12.010.
[72] S. de Valence, et al., Long term performance of polycaprolactone vascular grafts in a rat abdominal aorta replacement model, Biomaterials 33 (1) (2012) 38–47, https://doi.org/10.1016/j.biomaterials.2011.09.024.